iScience

CellPress
OPEN ACCESS

Article

Kaempferol attenuates hyperuricemia combined with gouty arthritis via urate transporters and NLRP3/NF-κB pathway modulation

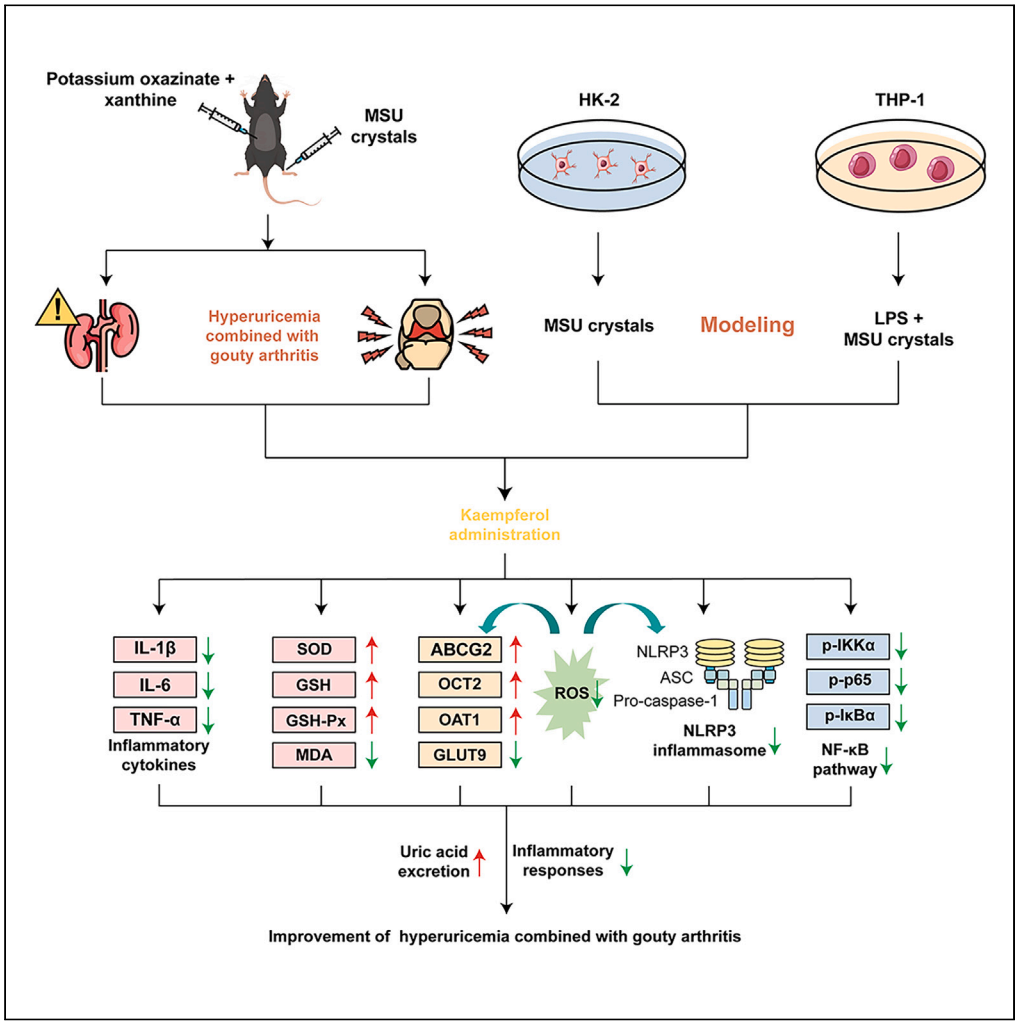

Yan Huang, Cantao Li, Wenjing Xu, ..., Yihuan Wang, Xiaoxi Zhang, Daozong Xia

xdz_zjtcm@hotmail.com

Highlights

Kaempferol (KPF) alleviates hyperuricemia and gouty arthritis in mouse models

KPF reduces oxidative stress and inflammation through NLRP3 inflammasome and NF-κB pathways

KPF modulates urate transporters, promoting uric acid excretion in mice

KPF inhibits ROS production, aiding in the regulation of ABCG2 and NLRP3 inflammasome

Huang et al., iScience 27, 111186
November 15, 2024
https://doi.org/10.1016/j.isci.2024.111186

iScience

CellPress
OPEN ACCESS

Article

Kaempferol attenuates hyperuricemia combined with gouty arthritis via urate transporters and NLRP3/NF-κB pathway modulation

Yan Huang,[1,3] Cantao Li,[1,3] Wenjing Xu,[1] Fenfen Li,[1] Ying Hua,[1] Changyu Xu,[1] Chenxi Wu,[1] Yihuan Wang,[1] Xiaoxi Zhang,[2] and Daozong Xia[1,4,*]

SUMMARY

Hyperuricemia (HUA), caused by purine disorders, can lead to gouty arthritis (GA). Kaempferol (KPF), a natural flavonoid, has anti-inflammatory properties, though its mechanism in treating HUA combined with GA remains unclear. This study used a mouse model of HUA combined with GA and *in vitro* models with HK-2 and THP-1 cells to explore KPF's effects. Cells were treated with KPF or inhibitors of ABCG2, ROS, NLRP3 inflammasome, and nuclear factor κB (NF-κB) pathway. Quantitative assays measured uric acid (UA), creatinine, oxidative stress biomarkers, and pro-inflammatory cytokines. Histopathological analyses showed KPF improved renal and joint inflammation caused by HUA and GA. KPF alleviated oxidative stress, reduced pro-inflammatory cytokines, and regulated UA levels through the modulation of urate transporters, NLRP3 inflammasome, and NF-κB pathway. KPF's actions, partly mediated by ROS reduction, suggest it is a promising candidate for treating HUA combined with GA.

INTRODUCTION

Hyperuricemia (HUA) is a major predisposing factor for gout.[1] With the continuous improvement of people's living conditions, the intakes of high-protein, high-fructose, and high-purine foods have increased. This has led to a rising incidence of HUA and its complication, gouty arthritis (GA), in the population. Furthermore, there is a discernible trend toward a decreasing age of onset for these conditions. NOD-like receptor protein 3 (NLRP3) inflammasome plays a crucial role in the pathogenesis of inflammation. The activation of it is widely believed to occur through two sequential steps, referred to as priming and assembly. The priming step is triggered by pattern recognition receptors such as Toll-like receptors (TLRs), which activates the signaling pathway mediated by nuclear factor κB (NF-κB).[2,3] In the activation step, various stimuli, such as extracellular ATP, mitochondrial DNA, and pathogen-related components, trigger the assembly of NLRP3 inflammasome complexes. This leads to generation of cleaved-caspase-1 (c-caspase-1) after the recruitment and activation of caspase-1, which cleaves pro-interleukin-1β (IL-1β) and pro-interleukin-18 (IL-18) to generate their mature forms. The releases of mature IL-1β and IL-18 trigger inflammatory responses.[4–6] Several studies have demonstrated that regulating NLRP3 inflammasome activation is a promising strategy for the treatment of HUA and GA. For instance, phloretin was shown to attenuate HUA-induced chronic renal dysfunction via inhibiting NLRP3 inflammasome activation.[7] In addition, gallic acid was reported to suppress GA by inhibiting NLRP3 inflammasome activation and pyroptosis.[8] Thus, inhibiting inflammation through regulating NLRP3 inflammasome serves as a potential strategy for the treatment of HUA and GA.

Currently, two primary types of animal models for gout have been recognized consisting of HUA models and GA models. HUA models have been established through the oral administration of a mixture of adenine and potassium oxonate (PO) or through a combination of peritoneal injection of PO and intragastric administration of hypoxanthine.[7,9] GA models, on the other hand, have been successfully established in previous studies by injecting with monosodium urate (MSU) crystals into ankle joints.[10,11] However, given that HUA and GA often occur simultaneously in patients, the development of a combined animal model for these conditions is currently lacking.

The majority of clinical therapeutic drugs currently available for the treatment of HUA and GA exhibit significant side effects. Allopurinol, a prototypical xanthine oxidase (XOD) inhibitor, is effective in only a fraction of patients with HUA and is associated with the risk of renal toxicity and hypersensitivity reactions.[12] Colchicine (Col), commonly prescribed to relieve GA symptoms, may have a stimulating effect on the gastrointestinal tract, leading to gastrointestinal bleeding.[13,14] Benzbromarone (Ben), used for treating both HUA and GA, is prescribed with caution due to its hepatotoxicity.[15] Therefore, there is an urgent need to identify a safe and effective approach for preventing and treating the combined manifestation of HUA and GA.

[1]School of Pharmaceutical Sciences, Zhejiang Chinese Medical University, Hangzhou, China
[2]Academy of Chinese Medical Sciences, Zhejiang Chinese Medical University, Hangzhou, China
[3]These authors contributed equally
[4]Lead contact
*Correspondence: xdz_zjtcm@hotmail.com
https://doi.org/10.1016/j.isci.2024.111186

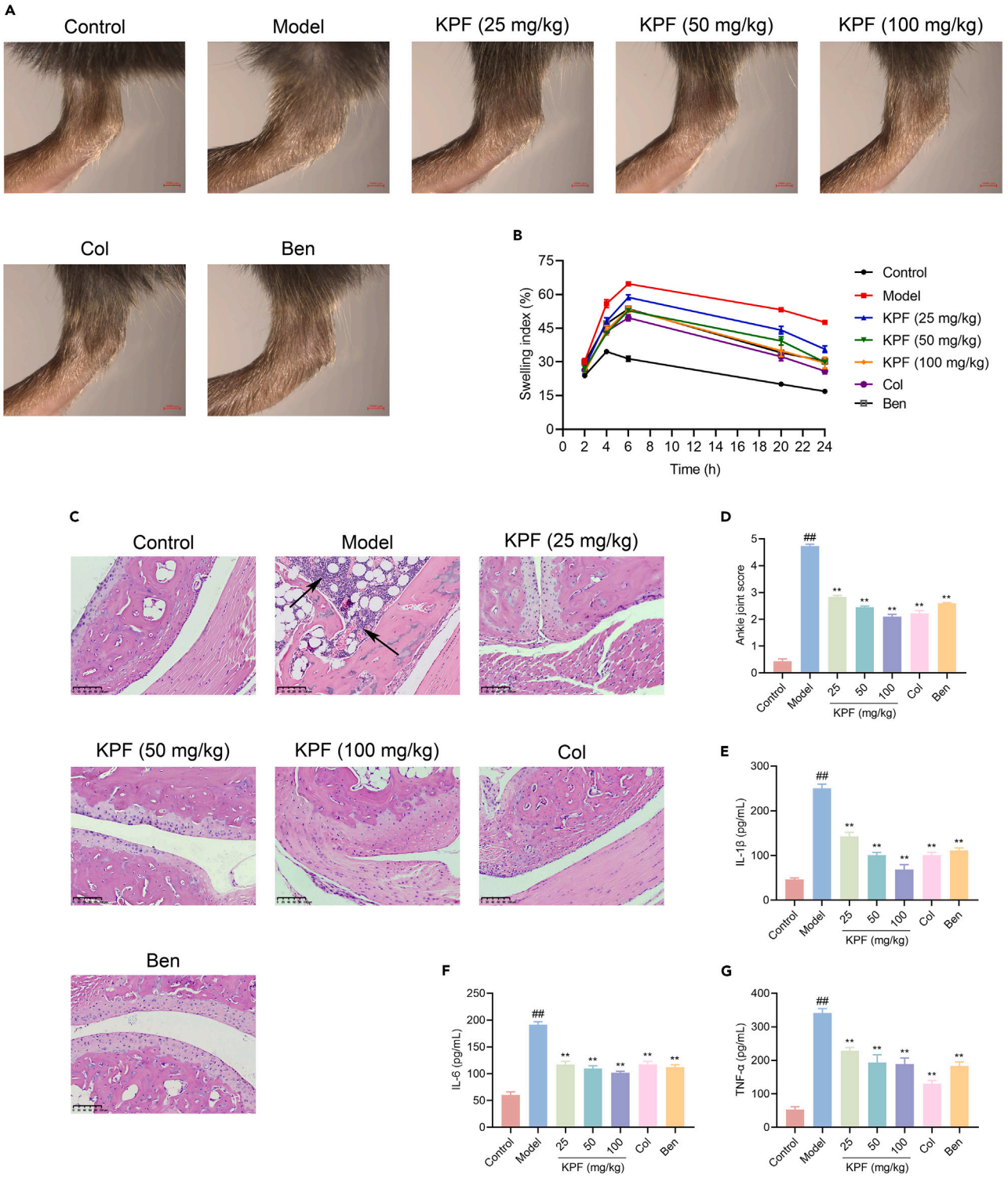

Figure 1. Effects of KPF on ankle swelling and inflammatory infiltration in mice

(A) Representative photographs of ankle joint swelling in mice 24 h after MSU injection. Scale bar, 1,000 μm.

(B) The tendency of swelling index in mice 24 h after MSU injection (n = 10 per group). The swelling index was subjected to calculations as described in the STAR Methods, and for data relating to swelling index, see Table S1.

(C) Representative H&E staining showing in ankle joints (the arrows indicate the infiltrating inflammatory cells). Scale bar, 100 μm.

Figure 1. *Continued*

(D) Histopathological score of ankle joints (n = 3 per group). The inflammatory infiltration of ankle joint was analyzed as described in the STAR Methods.

(E–G) The levels of IL-1β, IL-6, and TNF-α in ankle joints (n = 6 per group). Data for (D–G) are represented as mean ± SEM. One-way ANOVA followed by Dunnett's multiple comparisons test for (D–G). $^{\#\#}p < 0.01$ versus control group. $^{**}p < 0.01$ versus model group. IL-1β, interlukin-1β; IL-6, interlukin-6; TNF-α, tumor necrosis factor alpha; MSU, monosodium urate; KPF, kaempferol; Col, colchicine; Ben, benzbromarone.

In recent years, natural-products-based drugs have been considered a promising therapeutic strategy for preventing and treating inflammatory diseases. Among the various plant constituents in natural products, flavonoids, which are present in many herbal medicines and plant-based foods, are considered the most active compounds.[16] Kaempferol (KPF) is a widely occurring dietary bioflavonoid found in various fruits, vegetables, Chinese herbal medicines, and other natural plants, which has a range of pharmacological benefits including antioxidant and anti-inflammatory properties.[17–19] In particular, KPF has been found to exhibit reversible competitive inhibition of XOD activity, making it a potentially useful biological agent for treating HUA.[20] Therefore, this study attempted to investigate the protective effects of KPF on HUA combined with GA and reveal its underlying mechanism, in order to provide a basis for the development and application of KPF.

RESULTS

KPF alleviated ankle joint swelling and suppressed inflammatory infiltrations in mice

Initially, the most intuitive observation was that the degree of ankle joint swelling changed significantly under different interventions. Marked ankle joint swelling could be seen 2 h after MSU injection compared to control group, reaching the maximum at 6 h (Figure 1B; Table S1). Encouragingly, as shown in Figure 1A, after KPF treatment, the gouty symptoms were relieved, indicating that KPF could alleviate ankle joint swelling. Moreover, histological analysis of ankle joints showed that compared to control group, abundant inflammatory cell infiltrations were observed in model group. KPF treatment resulted in a significant reduction in the influx of inflammatory cells (Figure 1C). The mean ankle joint score of the mice in model group was significantly higher than that in control group ($p < 0.01$). After KPF administration, the mean scores of ankle joints in different groups were significantly decreased ($p < 0.01$), suggesting the reduced inflammatory infiltration caused by GA (Figure 1D). Since MSU has been reported to induce the expressions of inflammatory cytokines (IL-1β, IL-6, and tumor necrosis factor alpha [TNF-α]), leading to the aggravation of inflammatory reaction,[21,22] we further investigated the levels of IL-1β, IL-6 and TNF-α in ankle joints. As shown in Figures 1E–1G, significantly elevated levels of IL-1β, IL-6, and TNF-α were found after MSU injection compared to that of control group ($p < 0.01$). KPF treatment significantly reversed the elevations of IL-1β, IL-6, and TNF-α compared to model group in a dose-dependent manner ($p < 0.01$). All data showed that KPF could reduce the inflammatory cell infiltrations and inhibited cytokine productions in ankle joints.

KPF promoted UA excretion and reduced hepatic XOD activity in mice

As shown in Figures 2A and 2B, there were significant reductions in the levels of urine uric acid (UA) and creatinine (CRE) in model group when compared to those in control group ($p < 0.01$). Administration with KPF at 25, 50, and 100 mg/kg effectively increased the levels of urine UA and CRE compared to those of model group in a dose-dependent manner ($p < 0.01$). However, the levels of serum UA as well as indicators of renal function involving serum CRE and blood urea nitrogen (BUN) changed in the opposite direction (Figures 2C–2E). GFR is one of the important indexes to evaluate renal function. As shown in Figure 2F, GFR in model group was dramatically lower than that in control group ($p < 0.01$), whereas KPF treatment increased GFR significantly compared to model group ($p < 0.01$). In addition, the key enzyme XOD is closely related to the production of UA.[23,24] Hepatic XOD activity (Figure 2G) in mice of model group was evidently higher than that in control group ($p < 0.01$), whereas administration with KPF decreased hepatic XOD activity compared to mice in model group ($p < 0.01$).

KPF prevented renal dysfunction and alleviated histopathological changes in mice

Histological analysis through hematoxylin and eosin (H&E) staining provided insights into the renal tissue morphology. In control group, kidney tissues displayed a normal histological appearance. In contrast, model group exhibited distinct histological alterations characteristic of renal injury, including inconspicuous boundary between adjacent proximal tubule cells, glomerular atrophy, and tubular swelling. Remarkably, treatment with KPF effectively mitigated these histological changes (Figure 3A). As shown in Figure 3B, the mean kidney score of model group was significantly higher than that of control group ($p < 0.01$), suggesting that mice in model group appeared kidney injury. Meanwhile, the mean scores of kidneys in different KPF administration groups were significantly lower than those of model group ($p < 0.01$), indicating the improved renal tissue damage caused by HUA. Additionally, as shown in Figure 3C, it was not difficult to find an obvious production of IL-1β in model group in comparison to control group ($p < 0.01$). Nevertheless, KPF treatment could dose-dependently inhibit the production of IL-1β ($p < 0.01$).

The level of malondialdehyde (MDA), an oxidative stress marker, and the activities of antioxidative enzymes including superoxide dismutase (SOD), glutathione (GSH), and glutathione peroxidase (GSH-Px) were also measured (Figures 3D–3G). Compared with control group, obviously decreased activities of SOD, GSH, and GSH-Px and an increased level of MDA were observed in model group ($p < 0.01$). However, we observed that KPF reversed the reduction of SOD, GSH, and GSH-Px activities and the elevation of MDA level, especially for high-dose KPF treatment (100 mg/kg). These data demonstrated that KPF alleviated kidney oxidative stress.

KPF mitigated inflammatory injuries via downregulating NLRP3 inflammasome and NF-κB pathway in ankle joints of mice

In model group, the protein expressions of NLRP3, caspase-1, c-caspase-1 ASC, p-IKKα/IKKα, p-p65/p65, and p-IκBα/IκBα exhibited significant increases in comparison to control group (Figure 4). Following the administration of KPF, noticeable reductions in the protein

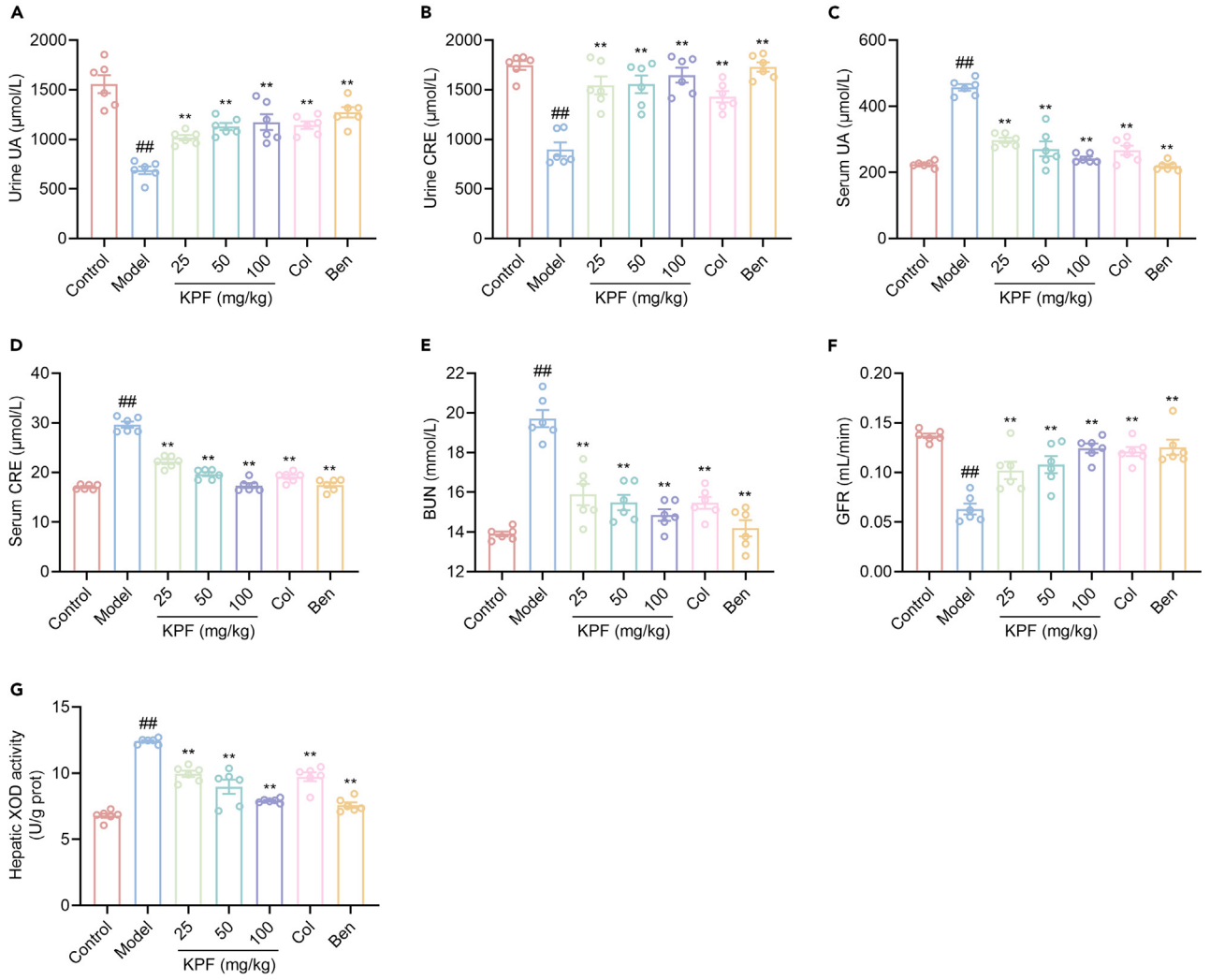

Figure 2. Effects of KPF on UA excretion and hepatic XOD activity in mice

(A–G) The results of urine UA, urine CRE, serum UA, serum CRE, BUN, GFR, and hepatic XOD activity in HUA combined with GA mice administered with various doses of KPF (20, 50, and 100 mg/kg) (n = 6 per group). Data for (A–G) are represented as mean ± SEM. One-way ANOVA followed by Dunnett's multiple comparisons test for (A–G). $^{\#\#}p < 0.01$ versus control group. $^{**}p < 0.01$ versus model group. HUA, hyperuricemia; GA, gouty arthritis; UA, uric acid; CRE, creatinine; BUN, blood urea nitrogen; XOD, xanthine oxidase; GFR, glomerular filtration rate. KPF, kaempferol; Col, colchicine; Ben, benzbromarone.

expressions of these aforementioned markers were observed when compared to model group. These evidences suggested that KPF possessed capabilities of alleviating inflammatory injuries of ankle joint through downregulating NLRP3 inflammasome and NF-κB pathway.

KPF regulated renal urate transporters, NLRP3 inflammasome, and NF-κB pathway in kidneys of mice

Renal-urate-transport-associated protein expressions were quantitatively detected by western blotting. As depicted in Figures 5A and 5B, model group exhibited a noteworthy down-regulation in the protein expressions of ABCG2, OCT2, and OAT1 compared to control group. Conversely, the protein expression of GLUT9 in model group was significantly up-regulated relative to control group. Remarkably, KPF treatment effectively mitigated these abnormal protein expressions, restoring levels of ABCG2, OAT1, OCT2, and GLUT9 in kidneys.

Furthermore, as mentioned earlier, KPF exhibited the capacity to reduce the level of inflammatory cytokine IL-1β in kidneys (Figure 3C). Notably, IL-1β represents one of the downstream products of NLRP3 and NF-κB inflammatory pathway.[25] Building upon these observations, our investigation extended to explore the impact of KPF on NLRP3 inflammasome and NF-κB pathway. As shown in Figures 5C–5F, the protein expressions of NLRP3, ASC, p-IKKα/IKKα, p-p65/p65, and p-IκBα/IκBα exhibited significant increases in kidneys of model group compared to control group. KPF treatment resulted in reductions in those protein expressions, suggesting the ability of KPF to suppress the activation of NLRP3 inflammasome and NF-κB pathway, thereby ameliorating kidney inflammation.

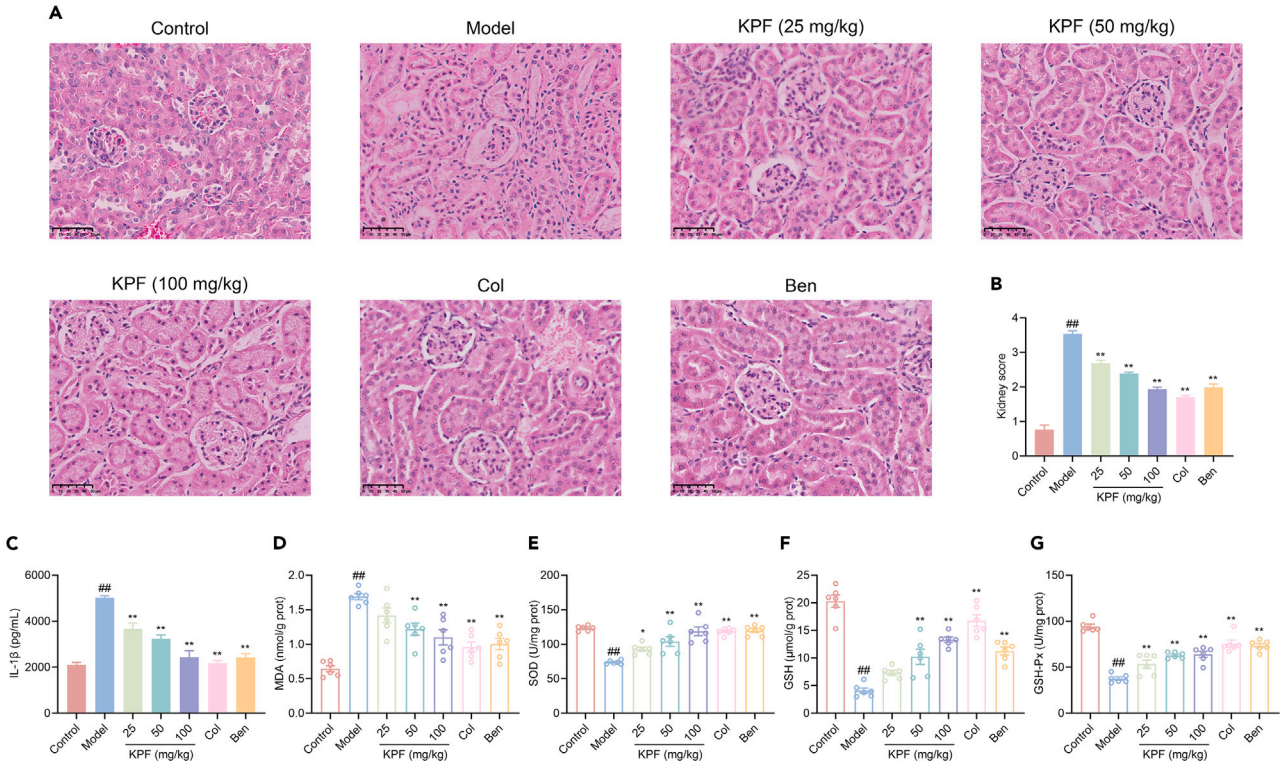

Figure 3. Effects of KPF on kidney inflammation and oxidative stress in mice

(A) Representative H&E staining in kidneys. Scale bar, 50 μm.

(B) Histopathological score of kidneys (n = 3 per group). The injury index of kidney was analyzed as described in the STAR Methods.

(C) The level of IL-1β in kidneys (n = 6 per group).

(D–G) The level of MDA and the activities of antioxidative enzymes including SOD, GSH, and GSH-Px in HUA combined with GA mice administered with various doses of KPF (20, 50, and 100 mg/kg) (n = 6 per group). Data for (B–G) are represented as mean ± SEM. One-way ANOVA followed by Dunnett's multiple comparisons test for (B–G). $^{\#\#}p < 0.01$ versus control group. $^{*}p < 0.05$, $^{**}p < 0.01$ versus model group. HUA, hyperuricemia; GA, gouty arthritis; IL-1β, interlukin-1β; MDA, malondialdehyde; SOD, superoxide dismutase; GSH, glutathione; GSH-Px, glutathione peroxidase; KPF, kaempferol; Col, colchicine; Ben, benzbromarone.

KPF improved MSU-induced damage in HK-2 cells and reduced LPS+MSU-induced inflammatory response in THP-1 cells

To elucidate the effects and underlying mechanism of KPF in reducing UA and exerting anti-inflammatory actions, *in vitro* investigations were conducted using HK-2 and THP-1 cells. According to the dosage screening by cell counting kit-8 (CCK-8), concentrations of 5 μM, 10 μM, and 20 μM of KPF were selected as the experimental concentrations for subsequent assays involving HK-2 and THP-1 cells (Figures S1A–S1D).

As observed in Figures 6A–6D, MDA level in MSU group exhibited a significant increase compared to control group ($p < 0.01$); conversely, SOD, GSH, and GSH-Px activities showed marked decreases in MSU group ($p < 0.01$), indicating that excessive UA induced damage to HK-2 cells and triggered oxidative stress. Following KPF treatment, MDA level significantly decreased ($p < 0.01$), and the activities of SOD, GSH, and GSH-Px remarkably increased when compared to MSU group ($p < 0.01$). The release of lactate dehydrogenase (LDH) is regarded as an important indicator of cell membrane integrity. Compared to control group, MSU stimulated HK-2 cells to release LDH (Figure 6E). After KPF treatment, a significant decrease in the level of LDH was observed ($p < 0.01$).

Additionally, Figures 6F–6H demonstrated notable elevations in the levels of inflammatory cytokines (IL-1β, IL-6, and TNF-α) in THP-1 cells after stimulation with LPS+MSU ($p < 0.01$). Encouragingly, KPF treatment resulted in significant reductions in IL-1β, IL-6, and TNF-α levels ($p < 0.01$).

KPF elevated ABCG2 in HK-2 cells and inhibited NLRP3 inflammasome and NF-κB pathway in THP-1 cells

Studies found that ABCG2 gene mutation exerts the greatest influence on human serum UA level by affecting its protein expression and the efficiency of UA transport.[26] Interventions were conducted in HK-2 cells using Ko143, recognized as one of the most effective functional inhibitors of ABCG2. As illustrated in Figures 7A and 7B, the observed upregulation of ABCG2 protein expression in response to the combined treatment with KPF and Ko143 suggested a potential role for these interventions in modulating the ABCG2 transporter. Results portrayed in Figures 7C–7F clearly demonstrated the suppressive effects of KPF, as well as inhibitors targeting NLRP3 inflammasome (MCC950) and NF-κB

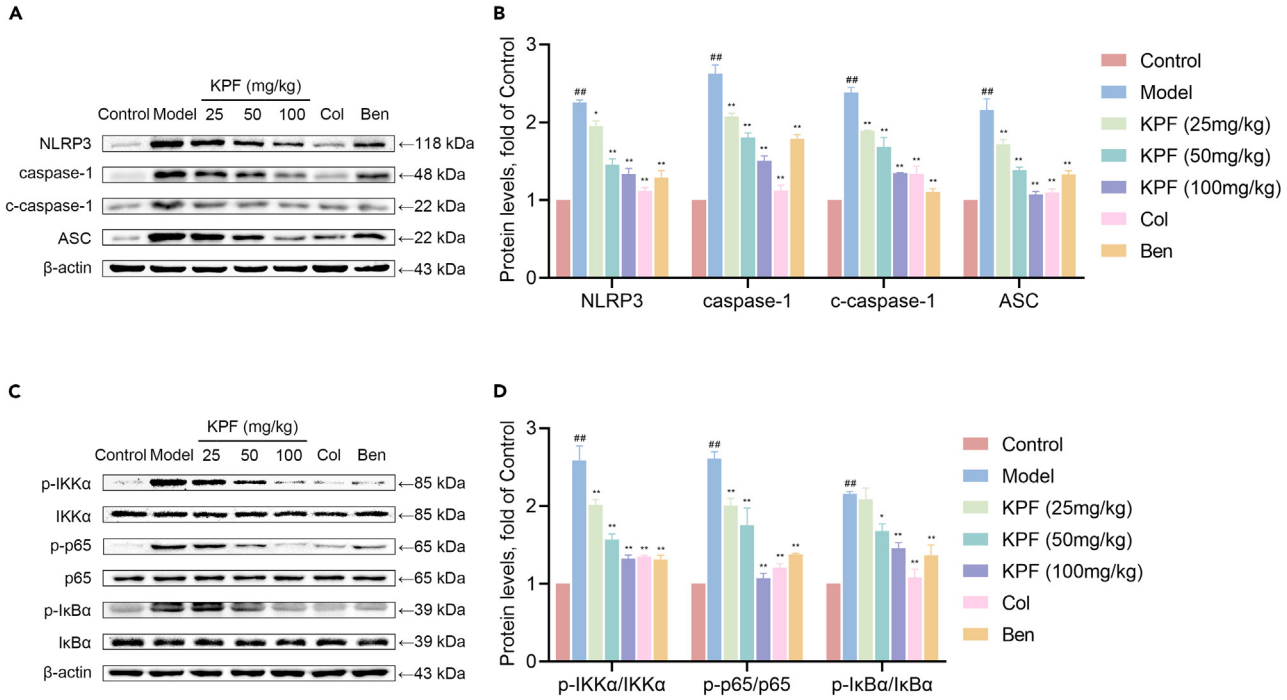

Figure 4. Effects of KPF on the protein expressions of NLRP3 inflammasome and NF-κB pathway in ankle joints

(A and B) Western blotting for NLRP3, caspase-1, c-caspase-1, and ASC and their quantification analysis (n = 3 per group). β-actin was used for internal normalization.

(C and D) Western blotting for p-IKKα, IKKα, p-p65, p65, p-IκBα, and IκBα and their quantification analysis (n = 3 per group). β-actin was used for internal normalization. Data for (B and D) are represented as mean ± SEM. One-way ANOVA followed by Dunnett's multiple comparisons test for (B and D). $^{\#\#}p < 0.01$ versus control group. $^{*}p < 0.05$, $^{**}p < 0.01$ versus model group. NLRP3, NOD-like receptor protein 3; c-caspase-1, cleaved-caspase-1; NF-κB, nuclear factor-kappa B; KPF, kaempferol; Col, colchicine; Ben, benzbromarone.

pathway (QNZ), on the expressions of key proteins involved in the signaling cascade, composing of NLRP3, caspase-1, c-caspase-1, ASC, p-IKKα, p-p65, and p-IκBα ($p < 0.01$).

KPF reduced the production of ROS to inhibit NLRP3 inflammasome and elevate ABCG2

The production of reactive oxygen species (ROS) is a critical second signal for the activation of NLRP3 inflammasome.[27] As shown in Figures 8A–8C, LPS+MSU stimulation led to a substantial increase in the production of ROS in THP-1 cells ($p < 0.01$). Treatments with both KPF and N-acetylcysteine (NAC) independently reduced the ROS generation. Moreover, the concomitant treatment with KPF and NAC resulted in a further diminution of ROS level. Accordingly, ROS stimulated by LPS+MSU significantly increased the protein expressions of NLRP3, c-caspase-1, and ASC compared with control group ($p < 0.01$). Both KPF and NAC treatment reversed this trend, and the combined treatment of the two further enhanced the effect against the expressions of these proteins (Figures 8D and 8E).

In HK-2 cells, stimulation with MSU significantly increased ROS production ($p < 0.01$). Treatment with either KPF or NAC alone effectively reduced ROS levels. Furthermore, the combined treatment with both KPF and NAC resulted in an even greater reduction in ROS levels (Figures 8F and 8G). The protein expression of ABCG2, a transporter responsible for the excretion of UA from the bloodstream into the urine, was notably decreased by MSU stimulation (Figures 8H and 8I). NAC, a radical scavenging accelerator, increased the expression of ABCG2, mirroring the effect of KPF. The combined use of NAC and KPF amplified this increase, demonstrating a more potent effect.

DISCUSSION

UA is a weak acid, and its ionized form presenting in the body is urate at physiologic pH.[28] The pathological threshold of HUA is defined as 6.8 mg/dL (the *in vitro* solubility limit of MSU).[29] When the level of serum UA is higher than the normal threshold, MSU crystal deposition begins to occur in tissues. Particularly, when the deposition of MSU crystal occurs in articular cartilage, synovial sacs, and other tissues, it will cause inflammation with concomitant swelling and pain, the process of which is called GA. It can be said that HUA is the most important risk factor for GA. The clinical picture of gout is divided into four stages: asymptomatic HUA, acute GA, intercritical period, and chronic tophaceous gout.[28] Several studies disclosed that MSU deposited in a proportion of asymptomatic HUA patients.[30,31] There are many separate animal models that have been widely developed to investigate the causal mechanisms for HUA or gout but do not yet reliably and

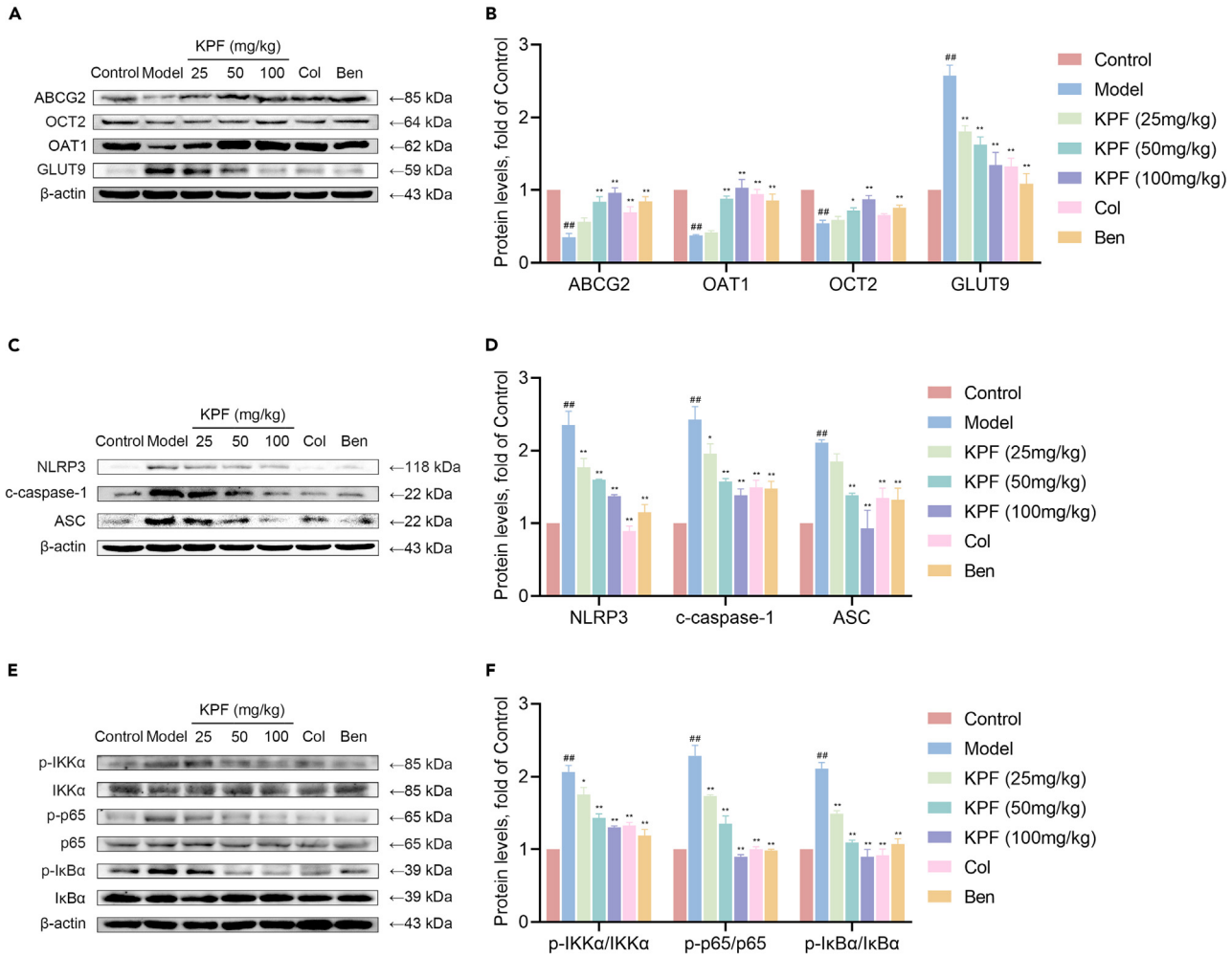

Figure 5. Effects of KPF on the protein expressions of renal urate transporters, NLRP3 inflammasome, and NF-κB pathway in kidneys

(A and B) Western blotting for ABCG2, OCT2, OAT1, and GLUT9 and their quantification analysis (n = 3 per group). β-actin was used for internal normalization. (C and D) Western blotting for NLRP3, c-caspase-1, and ASC and their quantification analysis (n = 3 per group). β-actin was used for internal normalization. (E and F) Western blotting for p-IKKα, IKKα, p-p65, p65, p-IκBα, and IκBα and their quantification analysis (n = 3 per group). β-actin was used for internal normalization. Data for (B, D, and F) are represented as mean ± SEM. One-way ANOVA followed by Dunnett's multiple comparisons test for (B, D, and F). $^{\#\#}p < 0.01$ versus control group. $^{*}p < 0.05$, $^{**}p < 0.01$ versus model group. ABCG2, ATP-binding cassette transporter G2; OCT2, organic cation transporter 2; OAT1, organic anion transporter 1; GLUT9, glucose transporter 9; NLRP3, NOD-like receptor protein 3; c-caspase-1, cleaved-caspase-1; NF-κB, nuclear factor κB ; KPF, kaempferol; Col, colchicine; Ben, benzbromarone.

simultaneously simulate HUA and its complication GA that occurs in humans. For protection, it is necessary to prevent UA from the formation of MSU crystal, which is effective in the treatment of gout. A combined HUA and GA animal model will be in line with the population in the transition stage from asymptomatic HUA to acute GA in clinical practice, which is a relatively practical application model. Therefore, this combined model possesses obvious research value and significance.

In present study, we successfully induced a mouse model of combined HUA and GA by combination of intraperitoneal injection of PO and xanthine, as well as intra-articular injection of MSU crystals.[10,11,32,33] As our data indicated, following KPF treatment, the photographs and H&E staining of ankle joints demonstrated similar changes that KPF significantly alleviated MSU-induced joint inflammation (ankle swelling and inflammatory cell infiltrations), mitigating symptoms of GA in mice. KPF could increase the excretion of UA and CRE in the kidney, as well as cause the levels of serum UA, CRE, and BUN tend to normal. Moreover, KPF improved kidney inflammation and showed a potential protective effect on renal injury by suppressing oxidative stress through activating the SOD, GSH, and GSH-Px and reducing MDA. In short, the remarkable improvement in biochemical parameters and histopathologic changes were observed after KPF treatment, indicating the urate-lowering and anti-inflammatory effects of KPF.

KPF could effectively lower UA level and might reduce UA production by inhibiting the activity of XOD. This inhibition could be attributed to the direct interaction between KPF and XOD, impeding its catalytic capacity in UA generation.[20] The transport and excretion of UA

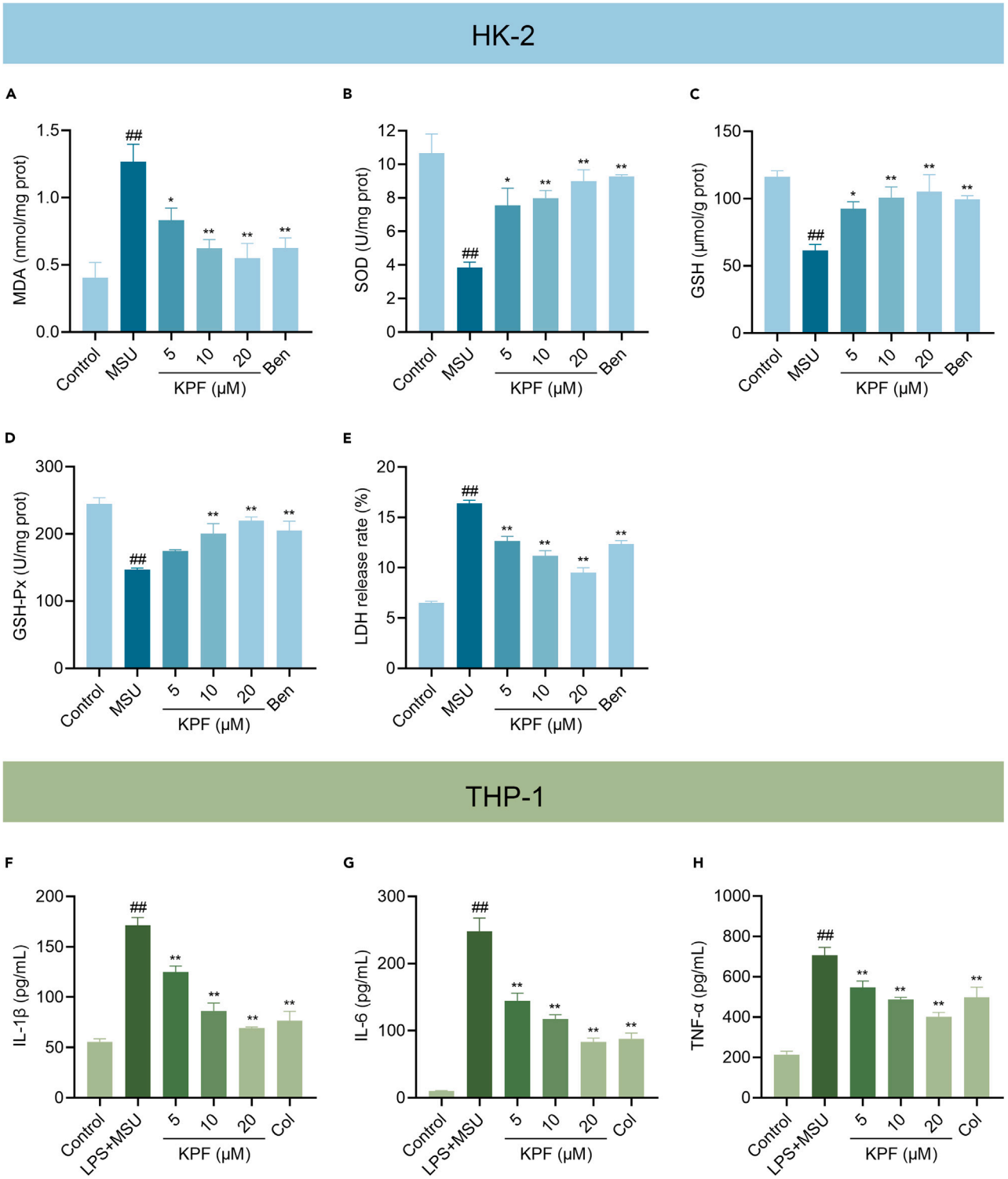

Figure 6. Effects of KPF on oxidative stress biomarkers and LDH in HK-2 cells and inflammatory cytokines in THP-1 cells

(A–D) The level of MDA and the activities of antioxidative enzymes including SOD, GSH, and GSH-Px in MSU-stimulated HK-2 cells administered with various doses of KPF (5, 10, and 20 μM) (n = 3 per group).

(E) The release rate of LDH in MSU-stimulated HK-2 cells administered with various doses of KPF (5, 10, and 20 μM) (n = 6 per group). The concentrations of KPF on HK-2 cells were selected using CCK-8, as shown in Figures S1A and S1B.

Figure 6. *Continued*

(F–H) The levels of IL-1β (n = 3 per group), IL-6 (n = 4 per group), and TNF-α (n = 4 per group) in LPS+MSU-stimulated THP-1 cells administered with various doses of KPF (5, 10, and 20 μM). The concentrations of KPF on THP-1 cells were selected using CCK-8, as shown in Figures S1C and S1D. Data for (A–H) are represented as mean ± SEM. One-way ANOVA followed by Dunnett's multiple comparisons test for (A–H). $^{\#\#}p < 0.01$ versus control group. $^{*}p < 0.05$, $^{**}p < 0.01$ versus MSU/LPS+MSU group. MDA, malondialdehyde; SOD, superoxide dismutase; GSH, glutathione; GSH-Px, glutathione peroxidase; LDH, lactate dehydrogenase; IL-1β, interlukin-1β; IL-6, interlukin-6; TNF-α, tumor necrosis factor-α; LPS, lipopolysaccharides; MSU, monosodium urate; KPF, kaempferol; Col, colchicine; Ben, benzbromarone.

are complicated procedures that are related with various renal transporters, including GLUT9, ABCG2, OAT1, OCT2, and so on.[34,35] According to previous studies, empagliflozin treatment was attributed to UA excretion promotion through up-regulating ABCG2 expression in KK-Ay mice with HUA.[9] Similarly, saponins induced the decrease of serum UA and increase of the excretion of urine UA through up-regulating the GLUT9 expression and down-regulating the OAT1 expression in chronic HUA rats.[36] Astaxanthin also promoted UA excretion by down-regulating the protein expressions of GLUT9, as well as up-regulating the protein expressions of OAT1 and ABCG2.[37] Consistent with previous findings, we found that KPF could effectively reverse the abnormal protein expressions of GLUT9, ABCG2, OAT1, and OCT2 in kidneys of mice. These results suggested that KPF might modulate urate transporters involved in UA metabolism and excretion.

Further molecular mechanisms *in vitro* revealed KPF's regulatory effects on UA metabolism pathways. ABCG2 is expressed in several organs critical for UA excretion, including the kidney and the intestine. In the kidney, ABCG2 is beneficial to excrete UA into urine, whereas in the intestine, it contributes to the excretion of UA into the gut for removal via the feces. This dual role enhances its influence on overall urate homeostasis.[38,39] Numerous genome-wide association studies have identified variants in the ABCG2 gene that are strongly associated with HUA and the risk of gout.[40,41] The findings from HK-2 cells demonstrated that the use of the ABCG2 inhibitor Ko143 effectively suppressed the function of ABCG2, thereby reducing the transport capacity of UA. This suggested that in the presence of Ko143, ABCG2 was unable to excrete UA normally, leading to an accumulation of UA within the cells. Subsequently, when Ko143 and KPF were applied to the cells together, KPF was able to increase the transport of UA and counteract the inhibitory effect of Ko143 on ABCG2. This further underscored that KPF regulated the urate transporters by activating or enhancing the function of ABCG2. KPF reportedly inhibited cancer cell growth by antagonizing estrogen receptor α and γ activities, and research suggested that the combination of estrogen and estrogen receptor α enhanced ABCG2 expression, indicating the potential role of estrogen receptor α on UA generation through ABCG2.[42,43] Based on the evidence mentioned earlier, it seems that KPF is likely to possess the ability to suppress the production of UA through estrogen receptor α regulating ABCG2. However, no research has been performed to verify this assumption.

Dysregulation of renal transporters can lead to excessive accumulation of UA in the body, which may activate inflammation. NLRP3 interacts with the bridging molecule ASC to increase the expression of caspase-1, which plays an important role in maturing IL-1β and IL-18 expressions.[44] NLRP3 inflammasome activation triggers inflammatory responses of kidney and joint along with the up-regulations of IL-1β and IL-18.[45,46] Moreover, NF-κB is produced by homologous or heterodimerization of Rel family proteins, mainly in the form of p50 and p65 subunits. Under normal conditions, NF-κB in the cytoplasm remains inactive and binds to the inhibitory protein IκB. Once stimulated, IκB kinase (IKK) is involved in the phosphorylation of IκBα, which then mediates the phosphorylation of NF-κB/p65.[47] The potential anti-inflammatory action of KPF may be exerted through direct or indirect influence on NLRP3 inflammasome and NF-κB pathway. KPF may directly inhibit the activity of key proteins in these pathways, such as NLRP3, caspase-1, c-caspase-1, ASC, p-IKKα, p-p65, and p-IκBα, thereby suppressing the inflammatory responses. Additionally, KPF might exert its anti-inflammatory effects by inhibiting signals that trigger the activation of NLRP3 inflammasome and NF-κB pathway, such as oxidative stress and pro-inflammatory cytokines. It is noteworthy that NLRP3 inflammasome and NF-κB pathways are interconnected in many respects.[48,49] MCC950, acting as a selective inhibitor of NLRP3 inflammasome, impeded the activation or perpetuation of its activated state, while not directly meddling with the priming process of NLRP3 inflammasome.[50] A study indicated that MCC950 might indirectly influence the priming phase of NLRP3 inflammasome via interaction and subsequent inhibition of the NF-κB/p65 molecule.[51] Given that NF-κB/p65 serves as a critical upstream signaling intermediary for NLRP3 inflammasome transcription, its inhibition could affect the expression level of NLRP3 inflammasome. We also conducted further investigations *in vitro*. Initially, KPF was found to reduce the expressions of protein associated with NLRP3 inflammasome or NF-κB pathway, but the bonding effect of NLRP3 inflammasome and NF-κB pathway inhibitors (MCC950 and QNZ) was comparable to that when combined with KPF intervention. This suggested that the anti-inflammatory action of KPF did not entirely depend on NLRP3 inflammasome or NF-κB pathway. Previous studies also have shown that mitogen-activated protein kinase (MAPK0, TLR4, and AR/NOX2 signaling pathways are involved in the antioxidant or anti-inflammatory process of KPF.[52,53] Interestingly, Ben, as a uricosuric agent rather than an anti-inflammatory, exerted an inhibitory action on NLRP3 inflammasome activation in this study. This could be attributed to the fact that Ben enhanced UA excretion and subsequently reduced the concentration of UA in the blood. This reduction potentially led to a decrease in MSU deposition, which in turn indirectly mitigated the activation of NLRP3 inflammasome.[54]

ROS functions as a second messenger to drive inflammasome activation and has been recognized as an important mechanism for the activation of NLRP3 inflammasome.[55] ROS can promote the activation of the inflammasome by oxidizing and modifying NLRP3 and other inflammasome components. For example, ROS can oxidize ASC, causing it to form ASC specks and bind to NLRP3, thus stimulating the assembly and activation of the inflammasome.[56] NAC, a potent ROS inhibitor, primarily replenishes intracellular GSH, a key antioxidant that neutralizes ROS to reduce cellular oxidative stress.[57] In this research, KPF was found to decrease ROS production, thereby inhibiting NLRP3 inflammasome. KPF's antioxidant effects may stem from its phenolic hydroxyl groups that trap ROS and prevent oxidative damage.[58,59] When

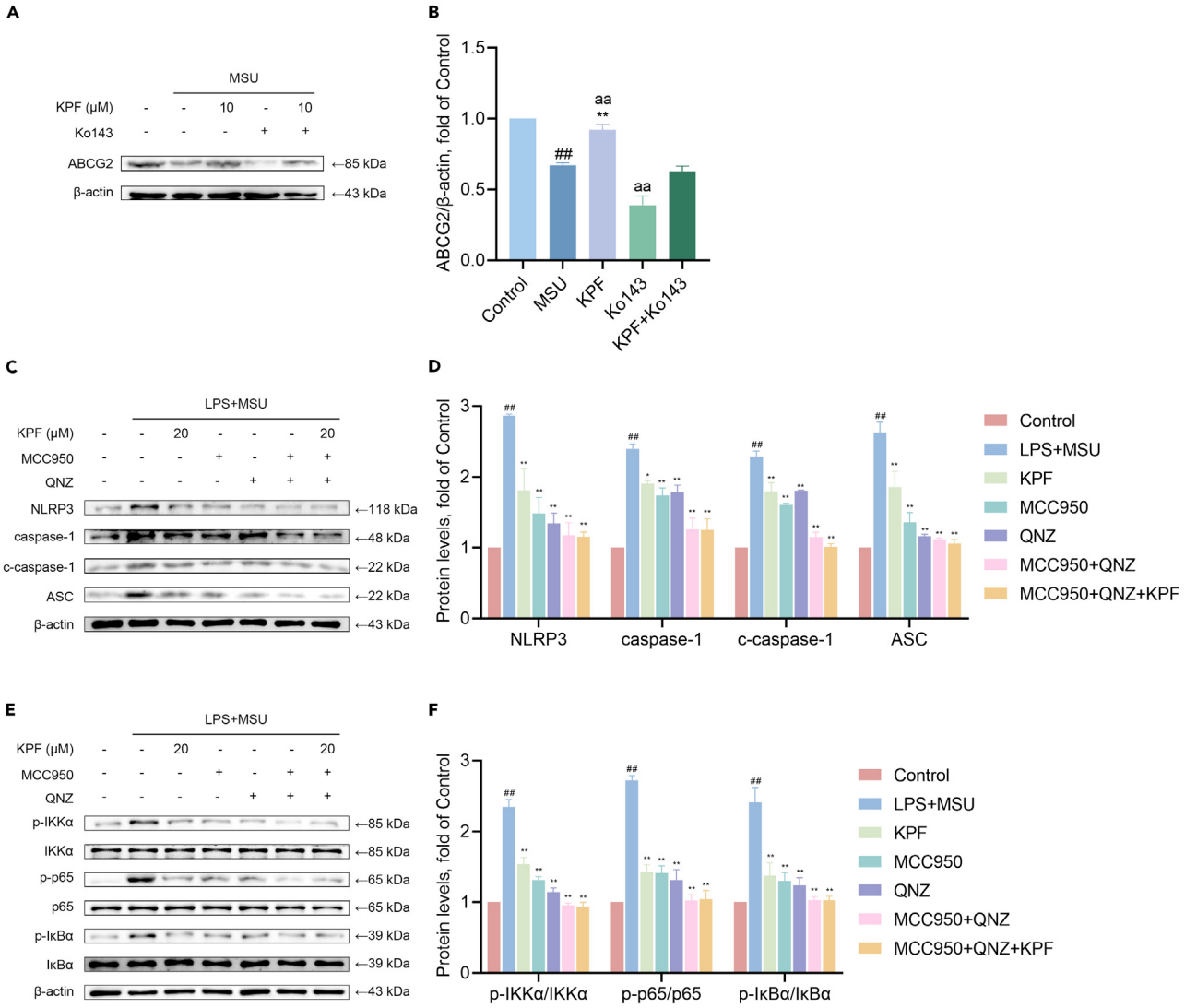

Figure 7. Effects of KPF on the protein expressions of ABCG2 in HK-2 cells and NLRP3 inflammasome and NF-κB pathway in THP-1 cells

(A and B) Western blotting for ABCG2 in HK-2 cells and its quantification analysis (n = 3 per group). β-actin was used for internal normalization.

(C and D) Western blotting for NLRP3, caspase-1, c-caspase-1, and ASC in THP-1 cells and their quantification analysis (n = 3 per group). β-actin was used for internal normalization.

(E and F) Western blotting for p-IKKα, IKKα, p-p65, p65, p-IκBα, and IκBα in THP-1 cells and their quantification analysis (n = 3 per group). β-actin was used for internal normalization. Data for (B, D, and F) are represented as mean ± SEM. One-way ANOVA followed by Dunnett's multiple comparisons test for (B, D, and F). $^{\#\#}p < 0.01$ versus control group. $^{*}p < 0.05$, $^{**}p < 0.01$ versus MSU/LPS+MSU group, $^{aa}p < 0.01$ versus KPF+Ko143 group. ABCG2, ATP-binding cassette transporter G2; NLRP3, NOD-like receptor protein 3; c-caspase-1, cleaved-caspase-1; NF-κB, nuclear factor κB; Ko143, ABCG2 inhibitor; MCC950, NLRP3 inflammasome inhibitor; QNZ, NF-κB pathway inhibitor; LPS, lipopolysaccharides; MSU, monosodium urate; KPF, kaempferol; Col, colchicine; Ben, benzbromarone.

combined, KPF and NAC synergistically combated ROS at different levels, enhancing the overall antioxidant effect. Additionally, ROS could potentially inflict direct damage to cellular structures through oxidative stress, including proteins and DNA. This could potentially inhibit the transcription and translation processes of ABCG2.[60] In this study, we investigated whether KPF can elevate ABCG2 expression by regulating ROS. Similar to the effects of NAC, the expression of ABCG2 was upregulated by KPF decreasing ROS production. The effect of ABCG2 on ROS production has also been previously reported. Inhibition of ABCG2 could increase intracellular ROS generation.[61,62]

In summary, KPF effectively ameliorated inflammation and reversed the abnormal expressions of renal transporter, leading to an increased excretion of UA. Our study demonstrated that KPF managed anti-inflammatory and urate-lowering effects through regulation of ROS-mediated renal transporters, NLRP3 inflammasome, and NF-κB pathway, highlighting its potential as a therapeutic agent for the treatment of HUA combined with GA.

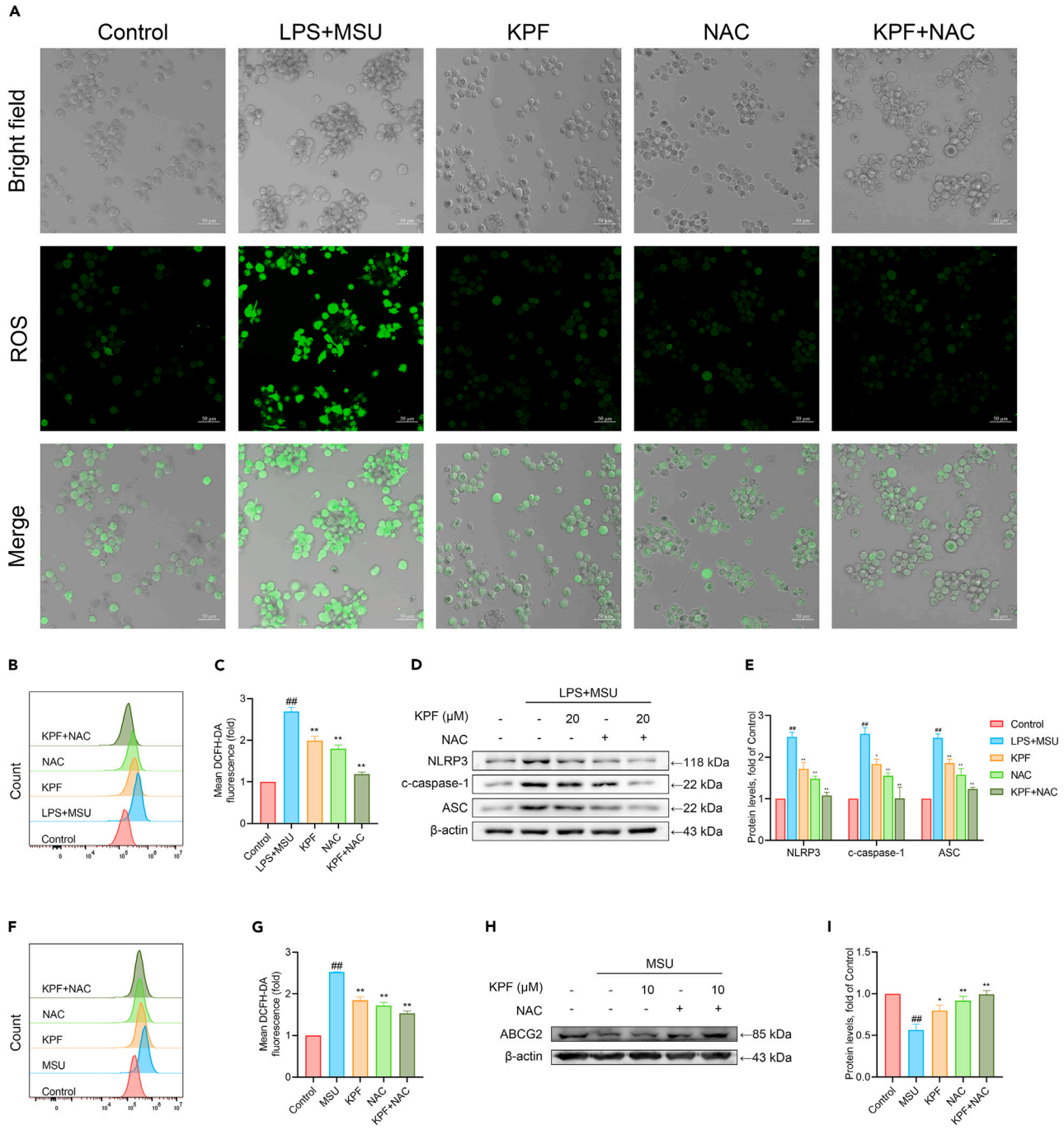

Figure 8. Effects of KPF on inhibiting NLRP3 inflammasome and elevating ABCG2 via the regulation of ROS

(A) CLSM images of THP-1 cells stained with DCFH-DA (green) for intracellular ROS detection. Scale bar, 50 μm.

(B and C) Flow cytometry detection of ROS production in THP-1 cells and their mean fluorescence intensity analysis (n = 3 per group).

(D and E) Western blotting for NLRP3, c-caspase-1, ASC in THP-1 cells and their quantification analysis (n = 3 per group). β-actin was used for internal normalization.

(F and G) Flow cytometry detection of ROS production in HK-2 cells and their mean fluorescence intensity analysis (n = 3 per group).

(H and I) Western blotting for ABCG2 in HK-2 cells and its quantification analysis. β-actin was used for internal normalization. Data for (C, E, G, and I) are represented as mean ± SEM. One-way ANOVA followed by Dunnett's multiple comparisons test for (C, E, G, and I). $^{\#\#}p < 0.01$ versus control group. $^{*}p < 0.05$, $^{**}p < 0.01$ versus MSU/LPS+MSU group. CLSM, confocal laser scanning microscopy; DCFH-DA, 2′,7′-dichlorodihydrofluorescein diacetate; NLRP3, NOD-like receptor protein 3; c-caspase-1, cleaved-caspase-1; ABCG2, ATP-binding cassette transporter G2; NAC, N-acetylcysteine; LPS, lipopolysaccharides; MSU, monosodium urate; KPF, kaempferol.

Limitations of the study

The limitation of the study in translating to human health comes from the differences between purine metabolism in humans and rodents. Rodents possess uricase enzymes, which catalyze the decomposition of UA, a capability that is absent in humans.[63] While rodents are often used as experimental models to study diseases related to purine metabolism, some of the findings may not be directly applicable to humans because of these differences. Moreover, when the serum UA level in the human body persistently surpasses the normal threshold, it leads to the deposition of MSU crystal in tissues such as the articular cartilage and synovial capsule, thereby initiating the development of GA. In mice, we established GA model by the injection of exogenous MSU crystal, which differs from the actual process of a GA flare in humans. Nevertheless, the lack of suitable *in vitro* cell model to simulate HUA combined with GA necessitates the segregation of our *in vitro* studies into distinct urate-lowering and anti-inflammatory models.

RESOURCE AVAILABILITY

Lead contact

Further information and requests for resources and reagents should be directed to and will be fulfilled by the lead contact, Daozong Xia (xdz_zjtcm@hotmail.com).

Materials availability

The study did not generate new unique reagents.

Data and code availability

All data reported in this paper will be shared by the lead contact upon request.

This paper does not report original code.

Any additional information required to reanalyze the data reported in this paper is avaliable from the lead contact upon request.

ACKNOWLEDGMENTS

This work was supported by National Natural Science Foundation of China (82074085, 82204726), Zhejiang Provincial Natural Science Foundation (LY21H280006, LQ22H280008), Opening Project of Zhejiang Provincial Preponderant and Characteristic Subject of Key University (Traditional Chinese Pharmacology) of Zhejiang Chinese Medical University (ZYAOXZD2019002), and Postgraduate Scientific Research Fund of Zhejiang Chinese Medical University (2021YKJ25, 2022YKJ20).

AUTHOR CONTRIBUTIONS

Y.H., conceptualization, investigation, methodology, and writing—original draft. C.T.L., conceptualization, data curation, and investigation. W.J.X., methodology, software, and visualization. F.F.L., funding acquisition and writing—review & editing. Y.H., data curation and visualization. C.Y.X., data curation and formal analysis. C.X.W., data curation and software. Y.H.W., data curation and resources. X.X.Z., funding acquisition, investigation, and validation. D.Z.X., conceptualization, funding acquisition, project administration, and writing—review & editing.

DECLARATION OF INTERESTS

The authors declare no competing interests.

STAR★METHODS

Detailed methods are provided in the online version of this paper and include the following:

- KEY RESOURCES TABLE
- EXPERIMENTAL MODEL AND SUBJECT DETAILS
  - Animals
  - Cell culture
- METHOD DETAILS
  - Establishment and treatment of a model combined HUA and GA
  - Measurement of ankle joint swelling
  - Serum, urine and liver biochemical analysis
  - Measurement of oxidative stress biomarkers in mice
  - Measurement of inflammatory cytokines in mice
  - Histopathological examination
  - Cell viability assay
  - Determination of oxidative stress biomarkers and LDH in HK-2 cells
  - Determination of inflammatory cytokines in THP-1 cells
  - Observation and determination of ROS production
  - Western blotting
- QUANTIFICATION AND STATISTICAL ANALYSIS

SUPPLEMENTAL INFORMATION

Supplemental information can be found online at https://doi.org/10.1016/j.isci.2024.111186.

Received: December 7, 2023
Revised: May 13, 2024
Accepted: October 14, 2024
Published: October 16, 2024

REFERENCES

1. Schlesinger, N., Norquist, J.M., and Watson, D.J. (2009). Serum urate during acute gout. J. Rheumatol. *36*, 1287–1289. https://doi.org/10.3899/jrheum.080938.
2. Bauernfeind, F.G., Horvath, G., Stutz, A., Alnemri, E.S., MacDonald, K., Speert, D., Fernandes-Alnemri, T., Wu, J., Monks, B.G., Fitzgerald, K.A., et al. (2009). Cutting edge: NF-kappaB activating pattern recognition and cytokine receptors license NLRP3 inflammasome activation by regulating NLRP3 expression. J. Immunol. *183*, 787–791. https://doi.org/10.4049/jimmunol.0901363.
3. Swanson, K.V., Deng, M., and Ting, J.P.Y. (2019). The NLRP3 inflammasome: molecular activation and regulation to therapeutics. Nat. Rev. Immunol. *19*, 477–489. https://doi.org/10.1038/s41577-019-0165-0.
4. Broz, P., von Moltke, J., Jones, J.W., Vance, R.E., and Monack, D.M. (2010). Differential requirement for Caspase-1 autoproteolysis in pathogen-induced cell death and cytokine processing. Cell Host Microbe *8*, 471–483. https://doi.org/10.1016/j.chom.2010.11.007.
5. Latz, E., Xiao, T.S., and Stutz, A. (2013). Activation and regulation of the inflammasomes. Nat. Rev. Immunol. *13*, 397–411. https://doi.org/10.1038/nri3452.
6. Renaudin, F., Orliaguet, L., Castelli, F., Fenaille, F., Prignon, A., Alzaid, F., Combes, C., Delvaux, A., Adimy, Y., Cohen-Solal, M., et al. (2020). Gout and pseudo-gout-related crystals promote GLUT1-mediated glycolysis that governs NLRP3 and interleukin-1β activation on macrophages. Ann. Rheum. Dis. *79*, 1506–1514. https://doi.org/10.1136/annrheumdis-2020-217342.
7. Cui, D., Liu, S., Tang, M., Lu, Y., Zhao, M., Mao, R., Wang, C., Yuan, Y., Li, L., Chen, Y., et al. (2020). Phloretin ameliorates hyperuricemia-induced chronic renal dysfunction through inhibiting NLRP3 inflammasome and uric acid reabsorption. Phytomedicine *66*, 153111. https://doi.org/10.1016/j.phymed.2019.153111.
8. Lin, Y., Luo, T., Weng, A., Huang, X., Yao, Y., Fu, Z., Li, Y., Liu, A., Li, X., Chen, D., and Pan, H. (2020). Gallic Acid Alleviates Gouty Arthritis by Inhibiting NLRP3 Inflammasome Activation and Pyroptosis Through Enhancing Nrf2 Signaling. Front. Immunol. *11*, 580593. https://doi.org/10.3389/fimmu.2020.580593.
9. Lu, Y.H., Chang, Y.P., Li, T., Han, F., Li, C.J., Li, X.Y., Xue, M., Cheng, Y., Meng, Z.Y., Han, Z., et al. (2020). Empagliflozin Attenuates Hyperuricemia by Upregulation of ABCG2 via AMPK/AKT/CREB Signaling Pathway in Type 2 Diabetic Mice. Int. J. Biol. Sci. *16*, 529–542. https://doi.org/10.7150/ijbs.33007.
10. Wu, C., Li, F., Zhang, X., Xu, W., Wang, Y., Yao, Y., Han, Z., and Xia, D. (2022). (-)-Epicatechin Ameliorates Monosodium Urate-Induced Acute Gouty Arthritis Through Inhibiting NLRP3 Inflammasome and the NF-κB Signaling Pathway. Front. Pharmacol. *13*, 799552. https://doi.org/10.3389/fphar.2022.799552.
11. Xu, W., Li, F., Zhang, X., Wu, C., Wang, Y., Yao, Y., and Xia, D. (2022). The Protective Effects of Neoastilbin on Monosodium Urate Stimulated THP-1-Derived Macrophages and Gouty Arthritis in Mice through NF-κB and NLRP3 Inflammasome Pathways. Molecules *27*, 3477. https://doi.org/10.3390/molecules27113477.
12. Pacher, P., Nivorozhkin, A., and Szabó, C. (2006). Therapeutic effects of xanthine oxidase inhibitors: renaissance half a century after the discovery of allopurinol. Pharmacol. Rev. *58*, 87–114. https://doi.org/10.1124/pr.58.1.6.
13. Schlesinger, N. (2017). The safety of treatment options available for gout. Expert Opin. Drug Saf. *16*, 429–436. https://doi.org/10.1080/14740338.2017.1284199.
14. Shi, Y., Cai, H., Niu, Z., Li, J., Pan, G., Tian, H., Wei, L., Chen, L., Yang, P., Wang, J., et al. (2021). Acute oral colchicine caused gastric mucosal injury and disturbance of associated microbiota in mice. Toxicology *461*, 152908. https://doi.org/10.1016/j.tox.2021.152908.
15. Azevedo, V.F., Kos, I.A., Vargas-Santos, A.B., da Rocha Castelar Pinheiro, G., and Dos Santos Paiva, E. (2019). Benzbromarone in the treatment of gout. Adv. Rheumatol. *59*, 37. https://doi.org/10.1186/s42358-019-0080-x.
16. Yi, Y.S. (2018). Regulatory Roles of Flavonoids on Inflammasome Activation during Inflammatory Responses. Mol. Nutr. Food Res. *62*, e1800147. https://doi.org/10.1002/mnfr.201800147.
17. Matei, I., and Hillebrand, M. (2010). Interaction of kaempferol with human serum albumin: a fluorescence and circular dichroism study. J. Pharm. Biomed. Anal. *51*, 768–773. https://doi.org/10.1016/j.jpba.2009.09.037.
18. Tsai, M.S., Wang, Y.H., Lai, Y.Y., Tsou, H.K., Liou, G.G., Ko, J.L., and Wang, S.H. (2018). Kaempferol protects against propacetamol-induced acute liver injury through CYP2E1 inactivation, UGT1A1 activation, and attenuation of oxidative stress, inflammation and apoptosis in mice. Toxicol. Lett. *290*, 97–109. https://doi.org/10.1016/j.toxlet.2018.03.024.
19. Choung, W.J., Hwang, S.H., Ko, D.S., Kim, S.B., Kim, S.H., Jeon, S.H., Choi, H.D., Lim, S.S., and Shim, J.H. (2017). Enzymatic Synthesis of a Novel Kaempferol-3-O-β-d-glucopyranosyl-(1→4)-O-α-d-glucopyranoside Using Cyclodextrin Glucanotransferase and Its Inhibitory Effects on Aldose Reductase, Inflammation, and Oxidative Stress. J. Agric. Food Chem. *65*, 2760–2767. https://doi.org/10.1021/acs.jafc.7b00501.
20. Wang, Y., Zhang, G., Pan, J., and Gong, D. (2015). Novel insights into the inhibitory mechanism of kaempferol on xanthine oxidase. J. Agric. Food Chem. *63*, 526–534. https://doi.org/10.1021/jf505584m.
21. Caution, K., Young, N., Robledo-Avila, F., Krause, K., Abu Khweek, A., Hamilton, K., Badr, A., Vaidya, A., Daily, K., Gosu, H., et al. (2019). Caspase-11 Mediates Neutrophil Chemotaxis and Extracellular Trap Formation During Acute Gouty Arthritis Through Alteration of Cofilin Phosphorylation. Front. Immunol. *10*, 2519. https://doi.org/10.3389/fimmu.2019.02519.
22. Oosterhuis, N.R., Fernandes, R., Maicas, N., Bae, S.E., Pombo, J., Gremmels, H., Poston, L., Joles, J.A., and Samuelsson, A.M. (2017). Extravascular renal denervation ameliorates juvenile hypertension and renal damage resulting from experimental hyperleptinemia in rats. J. Hypertens. *35*, 2537–2547. https://doi.org/10.1097/hjh.0000000000001472.
23. Isaka, Y., Takabatake, Y., Takahashi, A., Saitoh, T., and Yoshimori, T. (2016). Hyperuricemia-induced inflammasome and kidney diseases. Nephrol. Dial. Transplant. *31*, 890–896. https://doi.org/10.1093/ndt/gfv024.
24. Si, Y., Park, J.W., Jung, S., Hwang, G.S., Goh, E., and Lee, H.J. (2018). Layer-by-layer electrochemical biosensors configuring xanthine oxidase and carbon nanotubes/graphene complexes for hypoxanthine and uric acid in human serum solutions. Biosens. Bioelectron. *121*, 265–271. https://doi.org/10.1016/j.bios.2018.08.074.
25. Ruiz, P.A., Morón, B., Becker, H.M., Lang, S., Atrott, K., Spalinger, M.R., Scharl, M., Wojtal, K.A., Fischbeck-Terhalle, A., Frey-Wagner, I., et al. (2017). Titanium dioxide nanoparticles exacerbate DSS-induced colitis: role of the NLRP3 inflammasome. Gut *66*, 1216–1224. https://doi.org/10.1136/gutjnl-2015-310297.
26. Ohashi, Y., Kuriyama, S., Nakano, T., Sekine, M., Toyoda, Y., Nakayama, A., Takada, T., Kawamura, Y., Nakamura, T., Matsuo, H., et al. (2023). Urate Transporter ABCG2 Function and Asymptomatic Hyperuricemia: A Retrospective Cohort Study of CKD Progression. Am. J. Kidney Dis. *81*, 134–144.e1. https://doi.org/10.1053/j.ajkd.2022.05.010.
27. Elsayed, S., and Elsaid, K.A. (2022). Protein phosphatase 2A regulates xanthine oxidase-derived ROS production in macrophages and influx of inflammatory monocytes in a murine gout model. Front. Pharmacol. *13*, 1033520. https://doi.org/10.3389/fphar.2022.1033520.
28. Ragab, G., Elshahaly, M., and Bardin, T. (2017). Gout: An old disease in new perspective - A review. J. Adv. Res. *8*, 495–511. https://doi.org/10.1016/j.jare.2017.04.008.
29. Kim, I.Y., Han, K.D., Kim, D.H., Eun, Y., Cha, H.S., Koh, E.M., Lee, J., and Kim, H. (2019). Women with Metabolic Syndrome and General Obesity Are at a Higher Risk for Significant Hyperuricemia Compared to Men. J. Clin. Med. *8*, 837. https://doi.org/10.3390/jcm8060837.
30. Bardin, T., and Richette, P. (2014). Definition of hyperuricemia and gouty conditions. Curr. Opin. Rheumatol. *26*, 186–191. https://doi.org/10.1097/bor.0000000000000028.
31. Chen-Xu, M., Yokose, C., Rai, S.K., Pillinger, M.H., and Choi, H.K. (2019). Contemporary Prevalence of Gout and Hyperuricemia in the United States and Decadal Trends: The

National Health and Nutrition Examination Survey, 2007-2016. Arthritis Rheumatol. *71*, 991–999. https://doi.org/10.1002/art.40807.

32. Chen, J., Xu, L., Jiang, L., Wu, Y., Wei, L., Wu, X., Xiao, S., Liu, Y., Gao, C., Cai, J., and Su, Z. (2021). Sonneratia apetala seed oil attenuates potassium oxonate/hypoxanthine-induced hyperuricemia and renal injury in mice. Food Funct. *12*, 9416–9431. https://doi.org/10.1039/d1fo01830b.
33. Yong, T., Zhang, M., Chen, D., Shuai, O., Chen, S., Su, J., Jiao, C., Feng, D., and Xie, Y. (2016). Actions of water extract from Cordyceps militaris in hyperuricemic mice induced by potassium oxonate combined with hypoxanthine. J. Ethnopharmacol. *194*, 403–411. https://doi.org/10.1016/j.jep.2016.10.001.
34. Maiuolo, J., Oppedisano, F., Gratteri, S., Muscoli, C., and Mollace, V. (2016). Regulation of uric acid metabolism and excretion. Int. J. Cardiol. *213*, 8–14. https://doi.org/10.1016/j.ijcard.2015.08.109.
35. Wang, Z., Cui, T., Ci, X., Zhao, F., Sun, Y., Li, Y., Liu, R., Wu, W., Yi, X., and Liu, C. (2019). The effect of polymorphism of uric acid transporters on uric acid transport. J. Nephrol. *32*, 177–187. https://doi.org/10.1007/s40620-018-0546-7.
36. Zhu, L., Dong, Y., Na, S., Han, R., Wei, C., and Chen, G. (2017). Saponins extracted from Dioscorea collettii rhizomes regulate the expression of urate transporters in chronic hyperuricemia rats. Biomed. Pharmacother. *93*, 88–94. https://doi.org/10.1016/j.biopha.2017.06.022.
37. Le, Y., Zhou, X., Zheng, J., Yu, F., Tang, Y., Yang, Z., Ding, G., and Chen, Y. (2020). Anti-Hyperuricemic Effects of Astaxanthin by Regulating Xanthine Oxidase, Adenosine Deaminase and Urate Transporters in Rats. Mar. Drugs *18*, 610. https://doi.org/10.3390/md18120610.
38. Matsuo, H., Takada, T., Ichida, K., Nakamura, T., Nakayama, A., Ikebuchi, Y., Ito, K., Kusanagi, Y., Chiba, T., Tadokoro, S., et al. (2009). Common defects of ABCG2, a high-capacity urate exporter, cause gout: a function-based genetic analysis in a Japanese population. Sci. Transl. Med. *1*, 5ra11. https://doi.org/10.1126/scitranslmed.3000237.
39. Woodward, O.M., Köttgen, A., Coresh, J., Boerwinkle, E., Guggino, W.B., and Köttgen, M. (2009). Identification of a urate transporter, ABCG2, with a common functional polymorphism causing gout. Proc. Natl. Acad. Sci. USA *106*, 10338–10342. https://doi.org/10.1073/pnas.0901249106.
40. Dehghan, A., Köttgen, A., Yang, Q., Hwang, S.J., Kao, W.L., Rivadeneira, F., Boerwinkle, E., Levy, D., Hofman, A., Astor, B.C., et al. (2008). Association of three genetic loci with uric acid concentration and risk of gout: a genome-wide association study. Lancet *372*, 1953–1961. https://doi.org/10.1016/s0140-6736(08)61343-4.
41. Ichida, K., Matsuo, H., Takada, T., Nakayama, A., Murakami, K., Shimizu, T., Yamanashi, Y., Kasuga, H., Nakashima, H., Nakamura, T., et al. (2012). Decreased extra-renal urate excretion is a common cause of hyperuricemia. Nat. Commun. *3*, 764. https://doi.org/10.1038/ncomms1756.
42. Wang, H., Gao, M., and Wang, J. (2013). Kaempferol inhibits cancer cell growth by antagonizing estrogen-related receptor α and γ activities. Cell Biol. Int. *37*, 1190–1196. https://doi.org/10.1002/cbin.10152.
43. Chang, F.W., Fan, H.C., Liu, J.M., Fan, T.P., Jing, J., Yang, C.L., and Hsu, R.J. (2017). Estrogen Enhances the Expression of the Multidrug Transporter Gene ABCG2-Increasing Drug Resistance of Breast Cancer Cells through Estrogen Receptors. Int. J. Mol. Sci. *18*, 163. https://doi.org/10.3390/ijms18010163.
44. Duewell, P., Kono, H., Rayner, K.J., Sirois, C.M., Vladimer, G., Bauernfeind, F.G., Abela, G.S., Franchi, L., Nuñez, G., Schnurr, M., et al. (2010). NLRP3 inflammasomes are required for atherogenesis and activated by cholesterol crystals. Nature *464*, 1357–1361. https://doi.org/10.1038/nature08938.
45. Chen, Z., Zhong, H., Wei, J., Lin, S., Zong, Z., Gong, F., Huang, X., Sun, J., Li, P., Lin, H., et al. (2019). Inhibition of Nrf2/HO-1 signaling leads to increased activation of the NLRP3 inflammasome in osteoarthritis. Arthritis Res. Ther. *21*, 300. https://doi.org/10.1186/s13075-019-2085-6.
46. Vilaysane, A., Chun, J., Seamone, M.E., Wang, W., Chin, R., Hirota, S., Li, Y., Clark, S.A., Tschopp, J., Trpkov, K., et al. (2010). The NLRP3 inflammasome promotes renal inflammation and contributes to CKD. J. Am. Soc. Nephrol. *21*, 1732–1744. https://doi.org/10.1681/asn.2010020143.
47. Mitchell, J.P., and Carmody, R.J. (2018). NF-κB and the Transcriptional Control of Inflammation. Int. Rev. Cell Mol. Biol. *335*, 41–84. https://doi.org/10.1016/bs.ircmb.2017.07.007.
48. Zhao, W., Ma, L., Cai, C., and Gong, X. (2019). Caffeine Inhibits NLRP3 Inflammasome Activation by Suppressing MAPK/NF-κB and A2aR Signaling in LPS-Induced THP-1 Macrophages. Int. J. Biol. Sci. *15*, 1571–1581. https://doi.org/10.7150/ijbs.34211.
49. Afonina, I.S., Zhong, Z., Karin, M., and Beyaert, R. (2017). Limiting inflammation-the negative regulation of NF-κB and the NLRP3 inflammasome. Nat. Immunol. *18*, 861–869. https://doi.org/10.1038/ni.3772.
50. Tapia-Abellán, A., Angosto-Bazarra, D., Martínez-Banaclocha, H., de Torre-Minguela, C., Cerón-Carrasco, J.P., Pérez-Sánchez, H., Arostegui, J.I., and Pelegrin, P. (2019). MCC950 closes the active conformation of NLRP3 to an inactive state. Nat. Chem. Biol. *15*, 560–564. https://doi.org/10.1038/s41589-019-0278-6.
51. Ismael, S., Nasoohi, S., and Ishrat, T. (2018). MCC950, the Selective Inhibitor of Nucleotide Oligomerization Domain-Like Receptor Protein-3 Inflammasome, Protects Mice against Traumatic Brain Injury. J. Neurotrauma *35*, 1294–1303. https://doi.org/10.1089/neu.2017.5344.
52. Yuan, P., Sun, X., Liu, X., Hutterer, G., Pummer, K., Hager, B., Ye, Z., and Chen, Z. (2021). Kaempferol alleviates calcium oxalate crystal-induced renal injury and crystal deposition via regulation of the AR/NOX2 signaling pathway. Phytomedicine *86*, 153555. https://doi.org/10.1016/j.phymed.2021.153555.
53. Zhong, X., Zhang, L., Li, Y., Li, P., Li, J., and Cheng, G. (2018). Kaempferol alleviates ox-LDL-induced apoptosis by up-regulation of miR-26a-5p via inhibiting TLR4/NF-κB pathway in human endothelial cells. Biomed. Pharmacother. *108*, 1783–1789. https://doi.org/10.1016/j.biopha.2018.09.175.
54. Huang, W., Jiao, S., Chen, S., Chen, Y., Yang, Z., Wang, W., Cao, Z., Li, Z., and Zhang, L. (2022). Design, synthesis, and biological studies of dual URAT1 inhibitor and FXR agonist based on benzbromarone. Bioorg. Med. Chem. *75*, 117073. https://doi.org/10.1016/j.bmc.2022.117073.
55. Yu, X., Lan, P., Hou, X., Han, Q., Lu, N., Li, T., Jiao, C., Zhang, J., Zhang, C., and Tian, Z. (2017). HBV inhibits LPS-induced NLRP3 inflammasome activation and IL-1β production via suppressing the NF-κB pathway and ROS production. J. Hepatol. *66*, 693–702. https://doi.org/10.1016/j.jhep.2016.12.018.
56. Liu, X., Li, M., Chen, Z., Yu, Y., Shi, H., Yu, Y., Wang, Y., Chen, R., and Ge, J. (2022). Mitochondrial calpain-1 activates NLRP3 inflammasome by cleaving ATP5A1 and inducing mitochondrial ROS in CVB3-induced myocarditis. Basic Res. Cardiol. *117*, 40. https://doi.org/10.1007/s00395-022-00948-1.
57. Rushworth, G.F., and Megson, I.L. (2014). Existing and potential therapeutic uses for N-acetylcysteine: the need for conversion to intracellular glutathione for antioxidant benefits. Pharmacol. Ther. *141*, 150–159. https://doi.org/10.1016/j.pharmthera.2013.09.006.
58. Simunkova, M., Barbierikova, Z., Jomova, K., Hudecova, L., Lauro, P., Alwasel, S.H., Alhazza, I., Rhodes, C.J., and Valko, M. (2021). Antioxidant vs. Prooxidant Properties of the Flavonoid, Kaempferol, in the Presence of Cu(II) Ions: A ROS-Scavenging Activity, Fenton Reaction and DNA Damage Study. Int. J. Mol. Sci. *22*, 1619. https://doi.org/10.3390/ijms22041619.
59. Chen, J., Zhong, H., Huang, Z., Chen, X., You, J., and Zou, T. (2023). A Critical Review of Kaempferol in Intestinal Health and Diseases. Antioxidants *12*, 1642. https://doi.org/10.3390/antiox12081642.
60. Kurokawa, H., Ito, H., Terasaki, M., and Matsui, H. (2019). Hyperthermia enhances photodynamic therapy by regulation of HCP1 and ABCG2 expressions via high level ROS generation. Sci. Rep. *9*, 1638. https://doi.org/10.1038/s41598-018-38460-z.
61. Nie, S., Huang, Y., Shi, M., Qian, X., Li, H., Peng, C., Kong, B., Zou, X., and Shen, S. (2018). Protective role of ABCG2 against oxidative stress in colorectal cancer and its potential underlying mechanism. Oncol. Rep. *40*, 2137–2146. https://doi.org/10.3892/or.2018.6594.
62. Wang, J., Xue, X., Fan, K., Liu, Q., Zhang, S., Peng, M., Zhou, J., and Cao, Z. (2020). Moderate hypoxia modulates ABCG2 to promote the proliferation of mouse spermatogonial stem cells by maintaining mild ROS levels. Theriogenology *145*, 149–157. https://doi.org/10.1016/j.theriogenology.2019.10.007.
63. Kratzer, J.T., Lanaspa, M.A., Murphy, M.N., Cicerchi, C., Graves, C.L., Tipton, P.A., Ortlund, E.A., Johnson, R.J., and Gaucher, E.A. (2014). Evolutionary history and metabolic insights of ancient mammalian uricases. Proc. Natl. Acad. Sci. USA *111*, 3763–3768. https://doi.org/10.1073/pnas.1320393111.
64. Yang, Q., Wang, Q., Deng, W., Sun, C., Wei, Q., Adu-Frimpong, M., Shi, J., Yu, J., and Xu, X. (2019). Anti-hyperuricemic and anti-gouty arthritis activities of polysaccharide purified from Lonicera japonica in model rats. Int. J. Biol. Macromol. *123*, 801–809. https://doi.org/10.1016/j.ijbiomac.2018.11.077.
65. Huang, Y., Wu, C.X., Guo, L., Zhang, X.X., and Xia, D.Z. (2022). Effects of polysaccharides-riched Prunus mume fruit juice concentrate on uric acid excretion and gut microbiota in

mice with adenine-induced chronic kidney disease. Curr. Res. Food Sci. *5*, 2135–2145. https://doi.org/10.1016/j.crfs.2022.10.028.

66. Inker, L.A., and Titan, S. (2021). Measurement and Estimation of GFR for Use in Clinical Practice: Core Curriculum 2021. Am. J. Kidney Dis. *78*, 736–749. https://doi.org/10.1053/j.ajkd.2021.04.016.
67. Yin, C., Liu, B., Wang, P., Li, X., Li, Y., Zheng, X., Tai, Y., Wang, C., and Liu, B. (2020). Eucalyptol alleviates inflammation and pain responses in a mouse model of gout arthritis. Br. J. Pharmacol. *177*, 2042–2057. https://doi.org/10.1111/bph.14967.
68. Pettit, A.R., Ji, H., von Stechow, D., Müller, R., Goldring, S.R., Choi, Y., Benoist, C., and Gravallese, E.M. (2001). TRANCE/RANKL knockout mice are protected from bone erosion in a serum transfer model of arthritis. Am. J. Pathol. *159*, 1689–1699. https://doi.org/10.1016/s0002-9440(10)63016-7.
69. Dai, D.F., Sasaki, K., Lin, M.Y., Smith, K.D., Nicosia, R.F., Alpers, C.E., and Najafian, B. (2015). Interstitial eosinophilic aggregates in diabetic nephropathy: allergy or not? Nephrol. Dial. Transplant. *30*, 1370–1376. https://doi.org/10.1093/ndt/gfv067.
70. Wang, X.J., Ni, X.Q., Zhao, S., Zhao, R.Z., Wang, X.H., Xia, S.J., Sun, X.W., and Zhuo, J. (2022). ROS-NLRP3 signaling pathway induces sterile inflammation after thulium laser resection of the prostate. J. Cell. Physiol. *237*, 1923–1935. https://doi.org/10.1002/jcp.30663.
71. Yeh, I.J., Wang, T.Y., Lin, J.C., Lin, T.J., Chang, J.S., Yen, M.C., Liu, Y.H., Wu, P.L., Chen, F.W., Shih, Y.L., and Peng, C.Y. (2019). Optimal Regimen of N-Acetylcysteine on Chromium-Induced Renal Cell Damage. Metabolites *9*, 172. https://doi.org/10.3390/metabo9090172.
72. Cao, W., Zhang, J., Yu, S., Gan, X., and An, R. (2024). N-acetylcysteine regulates oxalate induced injury of renal tubular epithelial cells through CDKN2B/TGF-β/SMAD axis. Urolithiasis *52*, 46. https://doi.org/10.1007/s00240-023-01527-2.
73. Howley, R., Mansi, M., Shinde, J., Restrepo, J., and Chen, B. (2020). Evaluation of aminolevulinic acid-mediated protoporphyrin IX fluorescence and enhancement by ABCG2 inhibitors in renal cell carcinoma cells. J. Photochem. Photobiol., B *211*, 112017. https://doi.org/10.1016/j.jphotobiol.2020.112017.
74. Zhang, Y., Lv, X., Hu, Z., Ye, X., Zheng, X., Ding, Y., Xie, P., and Liu, Q. (2017). Protection of Mcc950 against high-glucose-induced human retinal endothelial cell dysfunction. Cell Death Dis. *8*, e2941. https://doi.org/10.1038/cddis.2017.308.
75. Zhang, Y., Tan, X., Lin, Z., Li, F., Yang, C., Zheng, H., Li, L., Liu, H., and Shang, J. (2021). Fucoidan from Laminaria japonica Inhibits Expression of GLUT9 and URAT1 via PI3K/Akt, JNK and NF-κB Pathways in Uric Acid-Exposed HK-2 Cells. Mar. Drugs *19*, 238. https://doi.org/10.3390/md19050238.

STAR★METHODS

KEY RESOURCES TABLE

REAGENT or RESOURCE	SOURCE	IDENTIFIER
Antibodies		
Anti-NLRP3	Cell Signaling Technology	Cat# 15101; RRID: AB_2722591
Anti-ASC, mouse-specific	Cell Signaling Technology	Cat# 67824; RRID: AB_2799736
Anti-ASC, human-specific	Cell Signaling Technology	Cat# 13833; RRID: AB_2798325
Anti-caspase-1, mouse-specific	Cell Signaling Technology	Cat# 24232; RRID: AB_2890194
Anti-caspase-1, human-specific	Cell Signaling Technology	Cat# 3866; RRID: AB_2069051
Anti-cleaved-caspase-1, mouse-specific	Cell Signaling Technology	Cat# 89332; RRID: AB_2923067
Anti-cleaved-caspase-1, human-specific	Cell Signaling Technology	Cat# 4199; RRID: AB_1903916
Anti-*p*-IKKα	Cell Signaling Technology	Cat# 2697; RRID: AB_2079382
Anti-IKKα	Cell Signaling Technology	Cat# 2682; RRID: AB_2799606
Anti-*p*-p65	Cell Signaling Technology	Cat# 8242; RRID: AB_10859369
Anti-p65	Cell Signaling Technology	Cat# 3033; RRID: AB_331284
Anti-*p*-IκBα	Cell Signaling Technology	Cat# 2859; RRID: AB_561111
Anti-IκBα	Cell Signaling Technology	Cat# 4812; RRID: AB_10694416
Anti-ABCG2	Cell Signaling Technology	Cat# 42078; RRID: AB_2799211
Anti-β-actin	Cell Signaling Technology	Cat# 4970; RRID: AB_2223172
HRP-linked Goat Anti-Rabbit IgG	Cell Signaling Technology	Cat# 7074; RRID: AB_2099233
Anti-OAT1	Abcam	Cat# ab135924; RRID: AB_3492058
Anti-OCT2	Abcam	Cat# ab179808; RRID: AB_2889931
Anti-GLUT9	Abcam	Cat# ab223470; RRID: AB_2882749
HRP-conjugated Goat Anti-Mouse IgG	Signaling Antibody	Cat# L3032; RRID: AB_2722565
Chemicals, peptides, and recombinant proteins		
Kaempferol, HPLC≥98%	Yuanye Biotechnology	Cat# B21126
Kaempferol, 95%	Yuanye Biotechnology	Cat# S25632
Colchicine	Aladdin Bio-Chem Technology	Cat# C106738
Benzbromarone	Aladdin Bio-Chem Technology	Cat# B131634
Potassium oxonate	Sigma-Aldrich	Cat# 2207-75-2
Xanthine	Sigma-Aldrich	Cat# 69-89-6
Monosodium urate	Sigma-Aldrich	Cat# 1198-77-2
Phorbol 12-myristate 13-acetate (PMA)	Sigma-Aldrich	Cat# P1585
Lipopolysaccharides (LPS)	Sigma-Aldrich	Cat# L4391
Ko143	Med Chem Express	Cat# HY-10010
MCC950	Med Chem Express	Cat# HY-12815
QNZ	Med Chem Express	Cat# HY-13812
NAC	Med Chem Express	Cat# HY-B0215
RIPA lysis buffer	CW Bio Technology	Cat# CW2333
Protease inhibitor cocktail	CW Bio Technology	Cat# CW2200
Phosphatase inhibitor cocktail	CW Bio Technology	Cat# CW2383
Critical commercial assays		
Bicinchoninic Acid (BCA) Kit	Beyotime BioTechnology	Cat# P0011
ROS Assay Kit	Beyotime BioTechnology	Cat# S0033
LDH Cytotoxicity Assay Kit	Beyotime BioTechnology	Cat# C0017

(*Continued on next page*)

Continued

REAGENT or RESOURCE	SOURCE	IDENTIFIER
XOD Assay Kit	NJJCBIO	Cat# A002-1-1
CRE Assay Kit	NJJCBIO	Cat# C011-2-1
BUN Assay Kit	NJJCBIO	Cat# C013-2-1
MDA Assay Kit	NJJCBIO	Cat# A003-1-2
SOD Assay Kit	NJJCBIO	Cat# A001-1-2
GSH Assay Kit	NJJCBIO	Cat# A006-2-1
GSH-Px Assay Kit	NJJCBIO	Cat# A005-1-2
CCK-8 -WST	Biosharp Life Sciences	Cat# BS350A
Mouse IL-1β ELISA Kit	Boster Bio Technology	Cat# EK0394
Human IL-1β ELISA Kit	Boster Bio Technology	Cat# EK0392
Mouse TNF-α ELISA Kit	Boster Bio Technology	Cat# EK0527
Human TNF-α ELISA Kit	Boster Bio Technology	Cat# EK0525
Mouse IL-6 ELISA Kit	Boster Bio Technology	Cat# EK0411
Human IL-6 ELISA Kit	Boster Bio Technology	Cat# EK0410
Experimental models: Cell lines		
THP-1	Shanghai Cell Bank	Cat# TCHu57
HK-2	Shanghai Cell Bank	Cat# GNHu47
Experimental models: Organisms/strains		
C57BL/6 mice	Shanghai SLAC ANIMAL	N/A
Software and algorithms		
ImageJ	NIH	https://imagej.net/software/imagej/
GraphPad Prism (version 8.0.2)	GraphPad Software	https://www.graphpad.com/
Adobe Illustrator	Adobe	https://www.adobe.com/
FlowJo (version 10.6.2)	BD Biosciences	https://www.flowjo.com/

EXPERIMENTAL MODEL AND SUBJECT DETAILS

Animals

Male C57BL/6 mice, aged 6–8 weeks and weighting about 20 g, were purchased from Shanghai SLAC Laboratory Animals Co., Ltd. Mice were housed under standard laboratory conditions (12-h light/dark cycle, temperature of 22 ± 2°C, humidity of 50 ± 5%) and had free access to food and water at Zhejiang Chinese Medical University Laboratory Animal Research Center (Permit Number: SYXK 2018–0012). All experimental procedures followed the Guide for the Care and Use of Laboratory Animals of China and was approved by Animal Ethical and Welfare Committee of Zhejiang Chinese Medical University (Ethical Approval Number: 20180813–01). Mice were acclimatized for 7 days prior to the experiments.

Cell culture

Human renal tubular epithelial cells (HK-2) and human myeloid leukemia mononuclear cells (THP-1) were obtained from the Shanghai Cell Bank of the Chinese Academy of Sciences (Shanghai, China). HK-2 cells were cultivated in Dulbecco's Modified Eagle Medium/Nutrient Mixture F-12 (DMEM/F-12), while THP-1 cells were cultivated in Roswell Park Memorial Institute (RPMI) 1640 medium. The medium was supplemented with 10% fetal bovine serum (FBS), and 1% penicillin and streptomycin. The cell cultures were maintained in a humidified atmosphere with 5% CO_2 at 37°C. HK-2 cells were allowed to grow in the culture medium for 24 h, while THP-1 cells were differentiated into macrophages during a 48 h incubation with PMA at a concentration of 50 ng/mL, in preparation for subsequent experimental procedures.

METHOD DETAILS

Establishment and treatment of a model combined HUA and GA

Mice were randomly divided into seven groups: control group, model group, three different concentrations of FPF groups (25, 50 and 100 mg/kg, Col group (1 mg/kg) and Ben group (10 mg/kg). KPF groups, Col group and Ben group were treated with the corresponding concentrations of KPF (purity ≥95%), Col and Ben by intragastric administration, and control group and model group were administrated with the same amount of normal saline solution once per day for 14 days. Throughout this experimental period, all mice, excluding those in control group,

were intraperitoneally injected with PO and xanthine suspension (280 mg/kg), while control group received an equivalent volume of normal saline solution. On the 13th day, 25 μL MSU suspension (50 mg/mL) was injected into bilateral ankle joints of mice, occurring 1 h after intragastric administration, except for control group. Control group received an equivalent volume of normal saline solution during the same time frame.[64]

Measurement of ankle joint swelling

A reference line, positioned at 0.5 cm above the ankle, was consistently marked with a non-fading marker to serve as a standardized point of reference for the measurement of toe volume. The toe volume was assessed prior to model establishment, as well as at specific time points post-establishment (2, 4, 6, 20, and 24 h) employing a toe volume measuring device.[10,11] The obtained data was subjected to calculations as per the formula outlined below. It's noteworthy that the measurements were conducted by an investigator who was blinded to the assignment of treatments.

$$\text{Swelling index} = \frac{V_{\text{after injection}} - V_{\text{before injection}}}{V_{\text{before injection}}} \times 100\%$$

Serum, urine and liver biochemical analysis

At the end of treatment, six mice from each group were placed in individual metabolic cages for 24 h to facilitate the collection of urine specimens. Subsequently, these urine samples were subjected to centrifugation at 3000 rpm for 10 min at 4°C. Blood samples were obtained and allowed to incubate at room temperature for 1 h before undergoing centrifugation at 3500 rpm for 15 min at 4°C, which effectively separated serum from other components. Liver tissues were homogenized in normal saline solution to create a 10% (*w/v*) homogenate, followed by centrifugation at 3000 rpm for 10 min at 4°C to extract supernatant. BUN and CRE concentrations in serum and urine, as well as hepatic XOD activity were measured according to manufacturer's instructions. Serum and urine uric acid (UA) concentrations were determined employing the phosphotungstic acid method.[65] Glomerular filtration rate (GFR) was estimated by calculating CRE clearance, which was done by using 24 h urine volume and CRE concentrations in both serum and urine via the following formula.[66,67]

$$\text{GFR} = \frac{\text{urine CRE} \times \text{V24 h}}{1440 \times \text{serum CRE}}$$

Measurement of oxidative stress biomarkers in mice

Kidney tissues were homogenized to prepare a 10% (*w/v*) homogenate, and then centrifuged to obtain the supernatant. Subsequent assessments of MDA, SOD, GSH and GSH-Px level were detected by using commercial detection kits.

Measurement of inflammatory cytokines in mice

Ankle tissues were meticulously isolated from surrounding fur and muscle, and a 10% (*w/v*) homogenate of the tissue is prepared. In addition, a 10% (*w/v*) homogenate of kidney tissue is prepared. The suspension was subjected to centrifugation at 12000 rpm at 4°C for 10 min, resulting in the acquisition of the supernatant. ELISA was applied to ascertain the concentrations of articular IL-1β, IL-6, and TNF-α, as well as renal IL-1β. The procedures were carried out according to the manufacturer's protocols.

Histopathological examination

Both ankle and kidney tissues underwent a rigorous preservation process utilizing 4% paraformaldehyde at room temperature for 24 h. For ankle tissues, subsequent to fixation, they underwent a decalcification procedure involving ethylenediaminetetraacetic acid (EDTA). Following these preparatory steps, kidney and ankle tissues were embedded in paraffin and subsequently sliced into sections measuring 4 μm in thickness. These sections of tissue were stained with H&E for observation. Histopathological score was used to analyze the injury index of kidney and the inflammatory infiltration of ankle joint according to the standard.[68,69]

Cell viability assay

For cell experiments, KPF (purity ≥98%) was solubilized in dimethyl sulfoxide (DMSO) and prepared to the required concentrations using cell culture medium. These solutions were filtered through a 0.22 μm filter membrane. HK-2 cells and THP-1 cells were separately seeded into 96-well plates at the density of 5×10^3 cells/well and cultured in medium containing various concentrations KPF. Cell viability was measured after 24 h culture using CCK-8 cell proliferation assay kit. Subsequently, HK-2 cells were pre-protected with different concentrations of KPF and Ben (0.4 μM) for 2 h and then stimulated with MSU (400 μM) for 22 h. Similarly, THP-1 cells were stimulated with LPS (1 μg/mL) for 24 h, then pre-protected with different concentrations of KPF and Col (0.1 μM) for 2 h, and finally stimulated with MSU (500 μM) for 22 h. Cell viability was determined by CCK-8 assay kit.

Determination of oxidative stress biomarkers and LDH in HK-2 cells

HK-2 cells were initially seeded in 6-well plates at the density of 2×10^5 cells/well. They were exposed to different concentrations of KPF and Ben for 2 h and then stimulated with MSU. After an additional 22 h, the cell precipitates were collected for analysis. The levels of key biomarkers, including MDA, SOD, GSH and GSH-Px in HK-2 cells were quantified using specialized assay kits.

HK-2 cells were seeded in 96-well plates at the density of 5×10^3 cells/well. After being exposed to KPF and Ben, followed by stimulation with MSU, the supernatant from HK-2 was collected and used to detected the level of LDH to reflect lysis of HK-2 in accordance to manufacturer's instructions.

Determination of inflammatory cytokines in THP-1 cells

THP-1 cells were seeded in 12-well plates at the density of 3×10^5 cells/well. Subsequent to the stimulation with LPS, the cells were exposed to KPF at varying concentrations and Col for 2 h. The cells were exposed to MSU for an additional 22 h. The culture supernatants were carefully collected, and the quantifications of IL-1β, IL-6 and TNF-α levels were measured using ELISA kits according to the manufacturer's instructions.

Observation and determination of ROS production

THP-1 cells were pretreated with ROS inhibitor NAC (5 mM) for 30 min before stimulation with MSU and then incubated with DCFH-DA (1000:1) prepared in serum-free medium for 20 min.[70] The fluorescent images of the cells were observed and recorded using confocal laser scanning microscopy (CLSM). Subsequently, ROS production of cells was detected using flow cytometry after being collected and washed.

HK-2 cells were pretreated with or without NAC at a final concentration of 4 mM for 2 h, and the cells were treated with or without KPF for 2 h.[71,72] Following this, the cells were exposed to MSU for 22 h and incubated with DCFH-DA. Then the cells were collected and washed, and the production of ROS was detected by flow cytometry.

Western blotting

HK-2 cells were initially cultured in 6-well plates at the density of 2×10^5 cells/well, and were subsequently treated with KPF and Ko143 (1 μM) for 2 h.[73] Likewise, HK-2 cells were treated with NAC. Following the treatment, the cells were stimulated with MSU for an additional 22 h. Subsequently, the cells were collected.

THP-1 cells were cultured in 6-well plates at the density of 1×10^6 cells/well. After LPS stimulation, these cells were treated simultaneously with KPF, MCC950 (1 μM) and QNZ (10 nM) for 2 h, following which MSU was introduced to induce stimulation for 22 h.[74,75] Likewise, THP-1 cells were treated with NAC, followed by stimulation with MSU. The cells were then collected.

Proteins were extracted from tissues and cells using RIPA buffer containing 1% phosphatase inhibitor and protease inhibitor, and concentrations of total proteins were determined by using a BCA Protein Assay Kit. Proteins were denatured by being heated in a metal bath for 10 min at 100°C. Equal aliquots of proteins were separated on SDS-PAGE and transferred onto polyvinylidene fluoride membranes, followed by blocking with 5% (*w/v*) non-fat milk dissolved in TBST for 1 h at room temperature. The membranes were incubated with the primary antibodies over night at 4°C and secondary antibodies for 1 h at room temperature. Protein bands on the membranes were visualized through enhanced chemiluminescence reagents. The densitometric analysis of the bands was quantified using ImageJ software tools.

QUANTIFICATION AND STATISTICAL ANALYSIS

Data are represented as mean ± SEM. One-way analysis of variance (ANOVA) followed by Dunnett's multiple comparisons test is used to evaluate the differences across multiple groups. ImageJ software is used to perform analysis for western blotting results. FlowJo (version 10.6.2) software is used to analyze the flow cytometry data. GraphPad Prism (version 8.0.2) software is used to draw column graphs and perform all statistical analysis. The statistical details and number of samples for each experiment is noted in the figure legends. $p < 0.05$ is considered to represent statistical significance.